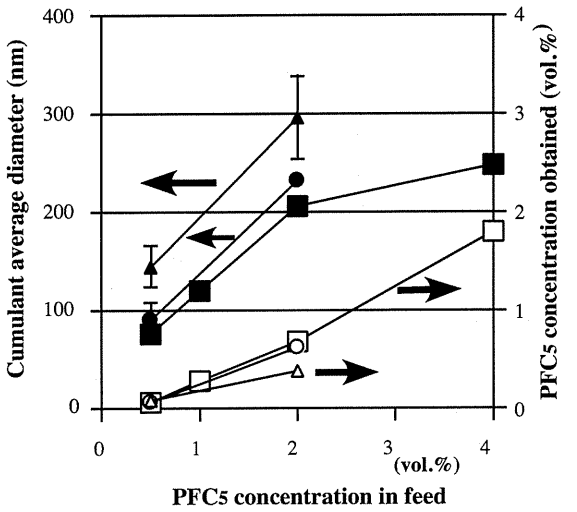

Fig. 4. Effects of polymer and PFC5 concentrations on physical properties of emulsions. PEG-P(Asp(C7F9)59) was used for emulsion preparations. Sample volume was 300 μL in 1.5-mL sample vials. Sonication was performed for 3 min at 40 °C. Filled plots represent cumulant average diameters, and vacant plots represent PFC5 concentrations of emulsions. Polymer concentration: △, ▲: 1.0 vol.%; ○, ●: 2.0 vol.%; □, ■: 4.0 vol.%.

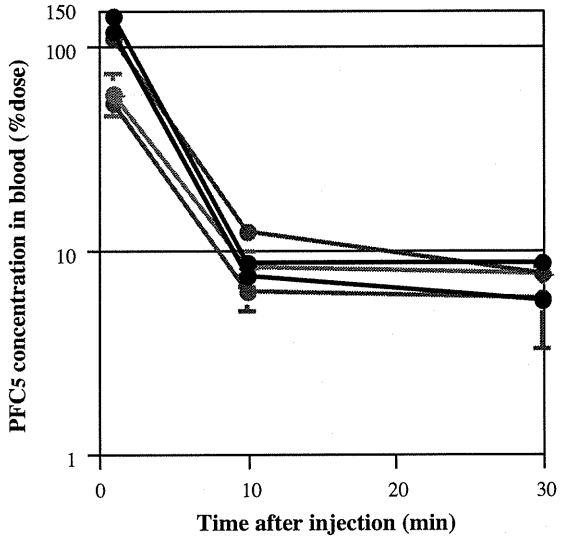

Fig. 5. Profiles of PFC5 concentration in blood. Black plot: run 1; blue plot: run 2; green plot: run 3; yellow plot: run 4; and red plot: run 5 (Table 5).

All these results indicate that the sonication method is a facile method for preparations of PFC5-containg emulsions with very small nano-sizes and high PFC5 concentrations.

3.3. *Effects of sample volume, polymer concentration, and PFC5 concentration on incorporation behaviors*

In the standard conditions, we put 300 μL water in a 1.5-mL of sealed glass tube and added polymer, PFC5, and PFC6. This configuration meant that a considerable amount of PFC5 perhaps would move from the solution into the glass tube's vacant atmospheric space (ca. 1.2 mL). We changed the volume of water while keeping constant the concentrations of polymer, PFC5, and PFC6 in the tube. Table 2 summarizes the results of runs 6–9 of Table 2. A higher PFC5 concentration was obtained in a case involving a larger water volume. (This means that there was a smaller vacant space in a sealed tube.) In accordance with the higher concentration of PFC5, the average diameter of the emulsion was observed to be larger. In run 9, PFC5's yield reached a very high value, approximately 90%. On the other hand, the PFC5's yield decreased to 32–33% when a small sample volume (300 μL) was adopted. These values indicate that the emulsification process can be well controlled through adjustment of sample volume.

Then, we examined effects that both polymer concentrations and PFC5 concentrations in feed had on the two physical values: diameter and PFC5 concentrations of the emulsion. Fig. 4 shows results of these two physical values for F-59% polymer cases. We changed the polymer concentration and the PFC5 concentration in feed in a range of 1.0–4.0 wt.% and of 0.5–4.0 vol.%, respectively. Each empty plot indicates PFC5 concentrations obtained for each polymer concentration, while each filled plot indicates cumulant average diameters for each polymer concentration. The polymer concentration was not found to significantly affect these two physical values. The polymer concentration affected very slightly the PFC5 content because three plot lines almost overlapped. When the polymer concentration was raised, only a small drop in the cumulant average diameter was observed. In contrast, the PFC5 concentration in feed was revealed to greatly affect the two physical values; larger values of PFC5 concentrations and cumulant average diameters were obtained with larger PFC5 concentrations in feed. Diameters of multi-modal distributions like Fig. 3(a) and (b) cannot be evaluated with the cumulant average diameters because the cumulant average diameters suppose the uni-modal diameter distribution. Therefore, we evaluated weight-weighted diameter distributions. Supplementary data, Table A summarizes and compares weight-weighted diameters with the cumulant average diameters. In most emulsion preparations, diameter distributions were found to be bi- or tri-modal, and therefore, exactly quantitative measurements of weight-weighted diameters are difficult in the homodyne analysis of dynamic light scattering done in this study. In fact, considerable differences are observed between the weight-weighted diameters and the cumulant average diameters for emulsions prepared in low PFC5 feed concentrations such as 1%, possibly due to the presence of empty polymeric micelles. (A DLS result of the empty micelle is shown in Fig. 3(c).) Even in this technical difficulty, the correlations obtained in Fig. 4a are not changed when multi-modal distributions are compared in the Supplementary data, Table A.

From the results obtained in this section, it was revealed that the sample volume and the PFC5 concentration in feed were appropriate factors for the facile control of size and the PFC5 content of the nano-sized emulsion.

3.4. *Function of PFC6 in an emulsion preparation*

In the above-described procedures for the emulsion preparation, we always used a 1:1 (vol./vol.) mixture of PFC5 and PFC6 in order to obtain a high PFC5 yield at a temperature higher than the boiling temperature of PFC5. We chose this 1:1 ratio because Kawabata et al. reported that ultrasound intensity required for the phase-transition (vaporization) induction at the 1:1 ratio was similar to that of a PFC5 alone case, and that this intensity was almost constant between ratios of 15:85, 50:50 (=1:1), and 85:15 (Asami et al., 2009). We varied temperatures (15, 25, 40, and 65 °C) of a sonicator's water bath, and performed the emulsion preparation both in the presence and the absence of PFC6 at each temperature. Table 3 summarizes results. In the absence of PFC6, PFC5 concentration was smaller than that of the corresponding PFC6-present case at every temperature. In runs 2 and 4, the obtained emulsions contained a considerable quantity of PFC5 over 0.2 vol.%. These two runs were prepared at lower temperatures than a boiling temperature of PFC5 (29 °C). Only a very small amount of PFC5

Table 3
Effects of temperature and PFC6 addition on PFC5 incorporation behaviors.

Run	Temperature (°C)	PFC6 addition	PFC5 concentration (vol.%)[a]	Cumulant average diameter (nm)[a]
1	15	Yes	0.727 ± 0.191	210.8 ± 17.8
2	15	No	0.419 ± 0.124	82.7 ± 2.6
3	25	Yes	0.566 ± 0.367	177.1 ± 8.9
4	25	No	0.205 ± 0.086	95.7 ± 8.9
5[b]	40	Yes	0.634 ± 0.361	173.5 ± 24.5
6	40	No	0.049 ± 0.059	98.5 ± 5.1
7	65	Yes	0.154 ± 0.051	136.2 ± 16.0
8	65	No	0.096[c]	303.7[c]

[a] Average ± standard deviation ($n = 3$) except run 8.
[b] This run is identical to run 6 of Table 2.
[c] Average of two preparations.

was incorporated in run 6, which was performed at 40 °C, which is above PFC5's boiling temperature. This indicates that most PFC5 evaporated at 40 °C, and that interfacial Laplace pressure did not suppress PFC5's evaporation in the sonication procedure possibly because PFC5 evaporated from macroscopic PFC's droplets (in mm scale) before its incorporation into nano-emulsions where Laplace pressure's effect is great. In contrast, the PFC6-present cases presented similar amounts of PFC5 incorporated at 15, 25, and 40 °C. This means that PFC5's evaporation at 40 °C was efficiently suppressed through the mixing with PFC6. PFC5 and PFC6 not only are miscible but also these two compounds are expected to strongly interact with each other because these are both perfluorocarbons. It is considered that PFC5 evades evaporation through the strong interaction with PFC6 that has a higher boiling temperature than 40 °C. In run 7, performed at 65 °C, a considerable drop in the incorporated PFC5 amount was seen. This sonication temperature (65 °C) is higher than PFC6's boiling temperature (60 °C), and therefore, both PFC5 and PFC6 were evaporated at 65 °C. From these results, we have confirmed the function of the added PFC6 for high PFC5-incorporation amounts at a temperature higher than PFC5's boiling temperature.

3.5. PFC5 concentration profile in blood

We measured PFC concentrations in blood using several PFC5-containing emulsions in order to control their pharmacokinetic behaviors. For a larger amount of emulsion accumulation at tumor tissues, a longer half-life is preferable for a contrast agent. In contrast, a shorter half-life is advantageous for a diagnosis in a short period after injection of a contrast injection, since a low concentration of the contrast agent in blood is a pre-requisite for a high contrast image of the contrast agent's accumulated region. Under this contradictory situation for the optimum half-life, it is very important to obtain technologies to control (prolong and shorten) a half-life of the contrast agent.

We used three different types of polymers including PEG-P(Asp(C7F9)x) block copolymers in order to control half-livers in blood. In Table 4, we describe the compositions of the two

Table 4
Compositions of two poly(L-lactic acid)(PLA)-containing polymers.

Code	Structure	Compositions
Gelatin derivative	Poly(L-lactic acid)-grafted gelatin	M.W. of PLA: 1000 weight ratio PLA/gelatin = 0.17
PEG-PLA	Poly(ethylene glycol)-b-Poly(L-lactic acid) Block copolymer	M.W. of PEG: 2000 M.W. of PLA: 1000

copolymers other than PEG-P(Asp(C7F9)x). These two copolymers contain hydrophobic poly(L-lactic acid) chains that are expected to work for incorporation of hydrophobic PFC5 into emulsions. Table 5 summarizes five samples prepared from four polymers. By adjusting the vacant volume of a 1.5-mL glass vial to a small value (ca., 300 μL, meaning 1.2 mL of the sample volume.), we successfully obtained emulsions with higher PFC5 contents than 0.4 vol.% in runs 1–3. In these cases, the sonication was carried out at 15 °C. When emulsions were prepared in the same conditions of run 1 except for a different temperature (at 40 °C) and a different vacant volume (ca. 0 μL), the PFC5 content was considerably lower (0.408 vol.%) than in run 1.

We injected these five samples in a mouse tail vein. As shown in Fig. 5, we observed a distinct difference in PFC5 concentrations at 1 min after the injection between three runs containing PLA (runs 1–3) and the other two runs for PEG-P(Asp(C7F9)x). The former three runs showed almost a 100% dose at 1 min with an assumption that blood volume was 7 vol./wt.% of body weight, while the latter two runs provided considerably smaller values than the 100% dose. In all runs, however, PFC5 concentrations were rapidly lowered at 10 and 30 min after the injection, and no clear difference was observed at these time points among all the runs. Therefore, control of pharmacokinetic behaviors, in particular prolongation of blood half-life from a few minutes, was not successfully achieved in this examination by the use of different polymer structures. For the pharmacokinetic control of the emulsions, an additional functional component may be required. Rapoport et al. (Rapoport et al., 2011) reported a very stable circulation (half-life = 2–4 h) in blood for perfluoro-crown-ether compound containing nano-emulsions.

Table 5
Compositions of PFC-emulsions for in vivo experiments.

Run	Polymer	Polymer concentration in feed (%)[a]	PFC5 concentration in feed (vol.%)	PFC5 concentration obtained in emulsion (vol.%)	Cumulant average diameter (nm)
1	Gelatin derivative[b]	1.0	1.25[d]	0.613	345.9
2	Gelatin derivative[b]	4.0	1.25[d]	0.429	542.6
3	PEG-b-PLA[a]	4.0	1.0[d]	0.491	222.6
4	F-15%[c]	4.0	2.0	0.465	256.3
5	F-59%[c]	4.0	1.0	0.670	225.1

[a] Weight (g)/water volume (mL).
[b] Listed in Table 4.
[c] Listed in Table 1.
[d] Sonication at 15 °C.

According to this report, a perfluoro compound showing stable emulsion formation may be utilized for stable incorporation of another PFC.

4. Discussion

In the examinations of this study, we successfully obtained very small (ca. 200 nm in diameter) PFC5-containing emulsions with high PFC5 contents in a very facile method using a common bath-type sonicator. Actually, the used sonicator was the smallest model with the lowest sonication power (max. Input power: 90 W) in its product line. The other facile aspect of this preparation method is the working temperature. By mixing PFC6 we performed the emulsion preparation at 40 °C, which is above the boiling temperature of PFC5. In a conventional method's use of a high-pressure emulsifier, cooling of the whole system is required for evading a large amount evaporation of PFC5 due to heat generated within a high-pressure emulsifier. In contrast, we did not need cooling samples during the preparation. This facileness is substantially important when we consider a scale-up of the emulsion preparations. In a large-scale production of these emulsions, the heat generated in preparation processes (both in emulsification and sonication) may become large enough to raise a temperature of the solution above the boiling temperature. Therefore, successful preparations at a high temperature means that there is a large margin for large-scale preparation with high PFC5 content as well as easy handling of samples at room temperature throughout the sonication procedure.

We could not substantially change pharmacokinetic behaviors of the PFC5-containing emulsion, even when using different polymers. This is a very different situation from polymeric micelle drug carrier cases where block polymer structure was revealed to be a very influential factor on pharmacokinetic behaviors of the incorporated drug into the polymeric micelles (Yokoyama, 2005, 2007; Watanabe et al., 2006). This difference may result from the liquid state of the emulsion's core, while the solid core is essential for stable drug incorporation in the polymeric micelle systems. An alternative and novel method may be required to obtain stable incorporation of liquid PFC for dramatically changed pharmacokinetics.

5. Conclusion

By using a bath-type sonicator, we successfully obtained PFC5-containing emulsions in a diameter range of 200 nm. These emulsions are very potent for theranostics of solid tumors through ultrasound irradiation. Furthermore, these emulsions were prepared in high PFC5 yields at 40 °C, which is higher than the boiling temperature of PFC5. This very facile preparation method is an important technological key for large-scale production of these medically valuable emulsions.

Acknowledgements

This work was supported by the New Energy and Industrial Technology Development Organization, Japan. M. Yokoyama, K. Shiraishi, and M. Nishihara acknowledge support from the JST CREST program, Grant-in-Aid of the Ministry of Education, Culture, Sports, Science and Technology, Japan, and Kanagawa Academy of Science and Technology. The authors acknowledge Dr. Kenichi Kawabata and Dr. Rei Asami of Central Research Laboratory, Hitachi, Ltd., for their valuable discussion on PFC-containing nanoemulsions.

Appendix A. Supplementary data

Supplementary data associated with this article can be found, in the online version, at doi:10.1016/j.ijpharm.2011.10.006.

References

Ai, H., 2011. Layer-by-layer capsules for magnetic resonance imaging and drug delivery. Adv. Drug Deliv. Rev. 63, 772–788.
Asami, R., Azuma, T., Kawabata, K., 2009. Fluorocarbon droplets as next generation contrast agents—their behavior under 1–3 mhz ultrasound. IEEE Proc. Int. Ultrasonics Symp., 1294–1297.
Asami, R., Ikeda, T., Azuma, T., Kawabata, K., Umemura, S., 2010. Acoustic signal characterization of phase change nanodroplets in tissue-mimicking phantom gels. Jpn. J. Appl. Phys. 49, 07HF16.
Blanco, E., Kessinger, C.W., Sumer, B.D., Gao, J., 2009. Multifunctional micellar nanomedicine for cancer therapy. Exp. Biol. Med. 234, 123–131.
Bryson, J.M., Fichter, K.M., Chu, W.J., Lee, J.H., Li, J., Madsen, L.A., McLendon, P.M., Reineke, T.M., 2009. Polymer beacons for luminescence and magnetic resonance imaging of DNA delivery. Proc. Natl. Acad. Sci. U.S.A. 106, 16913–16918.
Chen, X.S., 2011. Introducing theranostics journal—from the editor-in-chief. Theranostics 1, 1–2.
Gianella, A., Jarzyna, P.A., Mani, V., Ramachandran, S., Calcagno, C., Tang, J., Kann, B., Dijk, W.J., Thijssen, V.L., Griffioen, A.W., Storm, G., Fayad, Z.A., Mulder, W.J., 2011. A multifunctional nanoemulsion platform for imaging guided therapy evaluated in experimental cancer. ACS Nano 5, 4422–4433.
Grishenkov, D., Pecorari, C., Brismar, T.B., Paradossi, G., 2009. Characterization of acoustic properties of PVA-shelled ultrasound contrast agents: ultrasound-induced fracture (part II). Ultrasound Med. Biol. 35, 1139–1147.
Hernot, S., Klibanov, A.L., 2008. Microbubbles in ultrasound-triggered drug and gene delivery. Adv. Drug Deliv. Rev. 60, 1153–1166.
Ishida, O., Maruyama, K., Sasaki, K., Iwatsuru, M., 1999. Size-dependent extravasation and interstitial localization of polyethyleneglycol liposomes in solid tumor-bearing mice. Int. J. Pharm. 190, 49–56.
Jeong, H., Huh, M., Lee, S.J., Koo, H., Kwon, I.C., Jeong, S.Y., Kim, K., 2011. Photosensitizer-conjugated human serum albumin nanoparticles for effective photodynamic therapy. Theranostics 1, 230–239.
Kaida, S., Cabral, H., Kumagai, M., Kishimura, A., Terada, Y., Sekino, M., Aoki, I., Nishiyama, N., Tani, T., Kataoka, K., 2010. Visible drug delivery by supramolecular nanocarriers directing to single-platformed diagnosis and therapy of pancreatic tumor model. Cancer Res. 70, 7031–7041.
Kalber, T.L., Kamaly, N., Higham, S.A., Pugh, J.A., Bunch, J., McLeod, C.W., Miller, A.D., Bell, J.D., 2011. Synthesis and characterization of a theranostic vascular disrupting agent for in vivo MR imaging. Bioconjug. Chem. 22, 879–886.
Kamaly, N., Miller, A.D., 2010. Paramagnetic liposome nanoparticles for cellular and tumour imaging. Int. J. Mol. Sci. 11, 1759–1776.
Kawabata, K., Sugita, N., Yoshikawa, H., Azuma, T., Umemura, S., 2005. Nanoparticles with multiple perfluorocarbons for controllable ultrasonically induced phase shifting. Jpn. J. Appl. Phys. 44, 4548–4552.
Kawabata, K., Asami, R., Yoshikawa, H., Azuma, T., Umemura, S., 2010a. Acoustic response of microbubbles derived from phase-change nanodroplet. Jpn. J. Appl. Phys. 49, 07HF18.
Kawabata, K., Asami, R., Yoshikawa, H., Azuma, T., Umemura, S., 2010b. Sustaining microbubbles derived from phase change nanodroplet by low-amplitude ultrasound exposure. Jpn. J. Appl. Phys. 49, 07HF20.
Kim, K., Kim, J.H., Park, H., Kim, Y.S., Park, K., Nam, H., Lee, S., Park, J.H., Park, R.W., Kim, I.S., Choi, K., Kim, S.Y., Park, K., Kwon, I.C., 2010. Tumor-homing multifunctional nanoparticles for cancer theragnosis: simultaneous diagnosis, drug delivery, and therapeutic monitoring. J. Contr. Rel. 146, 219–227.
Lammers, T., Kiessling, F., Hennink, W.E., Storm, G., 2010. Nanotheranostics and image-guided drug delivery: current concepts and future directions. Mol. Pharm. 7, 1899–1912.
Lammers, T., Aime, S., Hennink, W.E., Storm, G., Kiessling, F., 2011. Theranostic Nanomedicines. Acc. Chem. Res. 44, 1029–1038.
Litzinger, D.C., Buiting, A.M.J., van Rooijen, N., Huang, L., 1994. Effect of liposome size on the circulation time and intraorgan distribution of amphipathic poly(ethylene glycol)-containing liposomes. Biochim. Biophys. Acta 1190, 99–107.
MacKay, J.A., Li, Z., 2010. Theranostic agents that co-deliver therapeutic and imaging agents? Adv. Drug Deliv. Rev. 62, 1003–1004.
Min, K.H., Kim, J.H., Bae, S.M., Shin, H., Kim, M.S., Park, S., Lee, H., Park, R.W., Kim, I.S., Kim, K., Kwon, I.C., Jeong, S.Y., Lee, D.S., 2010. Tumoral acidic pH-responsive MPEG-poly(beta-amino ester) polymeric micelles for cancer targeting therapy. J. Contr. Rel. 144, 259–266.
Mohan, P., Rapoport, N., 2010. Doxorubicin as a molecular nanotheranostic agent: effect of doxorubicin encapsulation in micelles or nanoemulsions on the ultrasound-mediated intracellular delivery and nuclear trafficking. Mol. Pharm. 6, 1959–1973.
Moon, G.D., Choi, S.W., Cai, X., Li, W., Cho, E.C., Jeong, U., Wang, L.V., Xia, Y., 2011. A new theranostic system based on gold nanocages and phase-change materials with unique features for photoacoustic imaging and controlled release. J. Am. Chem. Soc. 133, 4762–4765.
Nagayasu, A., Uchiyama, K., Nishida, T., Yamagiwa, Y., Kawai, Y., Kiwada, H., 1996. Is control of distribution of liposomes between tumors and bone marrow possible? Biochim. Biophys. Acta 1278, 29–34.
Nakamura, E., Makino, K., Okano, T., Yamamoto, T., Yokoyama, M., 2006. A polymeric micelle MRI contrast agent with changeable relaxivity. J. Contr. Rel. 114, 325–333.
Nishihara, M., Imai, K., Yokoyama, M., 2009. Preparation of perfluorocarbon/fluoroalkyl polymer nanodroplets for cancer-targeted ultrasound contrast agents. Chem. Lett. 38, 556–557.

Opanasopit, P., Yokoyama, M., Watanabe, M., Kawano, K., Maitani, Y., Okano, T., 2004. Block copolymer design for camptothecin incorporation into polymeric micelles for passive tumor targeting. Pharm. Res. 21, 2003–2010.

Pan, D., Caruthers, S.D., Hu, G., Senpan, A., Scott, M.J., Gaffney, P.J., Wickline, S.A., Lanza, G.M., 2008. Ligand-directed nanobialys as theranostic agent for drug delivery and manganese-based magnetic resonance imaging of vascular targets. J. Am. Chem. Soc. 130, 9186–9187.

Rapoport, N., Gao, Z., Kennedy, A., 2007. Multifunctional nanoparticles for combining ultrasonic tumor imaging and targeted chemotherapy. J. Natl. Cancer Inst. 99, 1095–1106.

Rapoport, N.Y., Kennedy, A.M., Shea, J.E., Scaife, C.L., Nam, K.H., 2009a. Controlled and targeted tumor chemotherapy by ultrasound-activated nanoemulsions/microbubbles. J. Contr. Rel. 138, 268–276.

Rapoport, N.Y., Nam, K.H., Gao, Z., Kennedy, A., 2009b. Application of ultrasound for targeted nanotherapy of malignant tumors. Acoust. Phys. 55, 594–601.

Rapoport, N., Christensen, D.A., Kennedy, A.M., Nam, K.H., 2010a. Cavitation properties of block copolymer stabilized phase-shift nanoemulsions used as drug carriers. Ultrasound Med. Biol. 36, 419–429.

Rapoport, N., Kennedy, A.M., Shea, J.E., Scaife, C.L., Nam, K.H., 2010b. Ultrasonic nanotherapy of pancreatic cancer: lessons from ultrasound imaging. Mol. Pharm. 7, 22–31.

Rapoport, N., Nam, K.H., Gupta, R., Gao, Z., Mohan, P., Payne, A., Todd, N., Liu, X., Kim, T., Shea, J., Scaife, C., Parker, D.L., Jeong, E.K., Kennedy, A.M., 2011. Ultrasound-mediated tumor imaging and nanotherapy using drug loaded, block copolymer stabilized perfluorocarbon nanoemulsions. J. Contr. Rel. 153, 4–15.

Sanson, C., Diou, O., Thévenot, J., Ibarboure, E., Soum, A., Brûlet, A., Miraux, S., Thiaudière, E., Tan, S., Brisson, A., Dupuis, V., Sandre, O., Lecommandoux, S., 2011. Doxorubicin loaded magnetic polymersomes: theranostic nanocarriers for MR imaging and magneto-chemotherapy. ACS Nano 5, 1122–1140.

Schutt, E.G., Klein, D.H., Mattrey, R.M., Riess, J.G., 2003. Injectable microbubbles as contrast agents for diagnostic ultrasound imaging: the key role of perfluorochemicals. Angew. Chem. Int. Ed. Engl. 42, 3218–3235.

Shiraishi, K., Kawano, K., Minowa, T., Maitani, Y., Yokoyama, M., 2009. Preparation and in vivo imaging of PEG-poly(L-lysine)-based polymeric micelle MRI contrast agents. J. Contr. Rel. 136, 14–20.

Shiraishi, K., Kawano, K., Maitani, Y., Yokoyama, M., 2010. Synthesis of Poly(ethylene glycol)-b-poly(L-lysine) block copolymers having Gd-DOTA as MRI contrast agent and their polymeric micelle formation by polyion complexation. J. Contr. Rel. 148, 160–167.

Solans, C., Izquierdo, P., Nolla, J., Azemar, N., Garcia-Celma, M.J., 2005. Nano-emulsions. Curr. Opin. Colloid Interface Sci. 10, 102–110.

Tadros, T., Izuquierdo, P., Esquena, J., Solans, C., 2004. Formation and stability of nano-emulsions. Adv. Colloid Interface. Sci. 108–109, 303–318.

Tanigo, T., Takaoka, R., Tabata, Y., 2010. Sustained release of water-insoluble simvastatin from biodegradable hydrogel augments bone regeneration. J. Contr. Rel. 143, 201–206.

Unger, E.C., Porter, T., Culp, W., Labell, R., Matsunaga, T., Zutshi, R., 2004. Therapeutic applications of lipid-coated microbubbles. Adv. Drug Deliv. Rev. 56, 1291–1314.

Yamamoto, T., Yokoyama, M., Opanasopit, P., Hayama, A., Kawano, K., Maitani, Y., 2007. What are determining factors for stable drug incorporation into polymeric micelle carriers? Consideration on physical and chemical characters of the micelle inner core. J. Contr. Rel. 123, 11–18.

Yokoyama, M., 2005. Polymeric micelles for the targeting of hydrophobic drugs. In: Kwon, G.S. (Ed.), Drug and Pharmaceutical Sciences, Polymeric Drug Delivery Systems, 148. Taylor & Francis, Boca Raton, pp. 533–575.

Yokoyama, M., 2007. Polymeric micelles as nano-sized drug carrier systems. In: Domb, A.J., Tabata, Y., Kumar, M.N.V.R., Farber, S. (Eds.), Nanoparticles for Pharmaceutical Applications. American Scientific Publishers, Stevenson Ranch, pp. 63–72.

Yokoyama, M., Opanasopit, P., Maitani, Y., Kawano, K., Okano, T., 2004. Polymer design and incorporation method for polymeric micelle carrier system containing water-insoluble anti-cancer agent camptothecin. J. Drug Target. 12, 373–384.

Yuan, F., Dellian, M., Fukumura, D., Leunig, M., Berk, D.A., Torchilin, V.P., Jain, R.K., 1995. Vascular permeability in a human tumor xenograft: molecular size dependence and cutoff size. Cancer Res. 55, 3752–3756.

Watanabe, M., Kawano, K., Yokoyama, M., Opanasopit, P., Okano, T., Maitani, Y., 2006. Preparation of camptothecin-loaded polymeric micelles and evaluation of their incorporation and circulation stability. Int. J. Pharm. 308, 183–189.

J Exp Clin Med 2011;3(4):151–158

Contents lists available at ScienceDirect

Journal of Experimental and Clinical Medicine

journal homepage: http://www.jecm-online.com

REVIEW ARTICLE

Clinical Applications of Polymeric Micelle Carrier Systems in Chemotherapy and Image Diagnosis of Solid Tumors

Masayuki Yokoyama*

Medical Engineering Laboratory, Research Center for Medical Science, The Jikei University School of Medicine, Tokyo, Japan

ARTICLE INFO

Article history:
Received: Jan 28, 2011
Revised: Apr 25, 2011
Accepted: Apr 29, 2011

KEY WORDS:
chemotherapy;
drug carriers;
image diagnosis;
polymeric micelles;
solid tumors

Polymeric micelles are assemblies of synthetic polymers and have been studied and developed as drug carriers for targeting solid tumors. Physicochemical characters and medical advantages of the polymeric micelle carrier systems are summarized, followed by an explanation of their recent application for contrast agent targeting. In the final section, future perspectives on the polymeric micelle carrier systems for tumor targeting are discussed, including a novel combination of contrast agent targeting and drug targeting that achieves tumor-specific image diagnosis and tumor-selective chemotherapy, respectively.

1. Polymeric Micelles as Nano-sized Drug Carriers[1–8]

In this review, I focused only on a brief explanation on fundamental aspects and on the present clinical situation of drug targeting with polymeric micelle carriers. The drug tumor targeting with polymeric micelle carriers has been attained first by Japanese researchers including the author of this review, and clinical trials of the polymeric micelle targeting had been started first in Japan. I do not describe recent developments of polymeric micelle carrier's research that must provide many references of non-Japanese groups. Therefore, a considerably large proportion of references in this review is written by Japanese groups. Please understand this situation, and if readers want to know recent developments of polymeric micelle drug carriers, please read other reviews.[1,2,4–8]

1.1. What is a polymeric micelle?

A polymeric micelle is a macromolecular assembly that forms from synthetic block copolymers or graft copolymers and that has a spherical inner core and an outer shell.[9] As shown in Figure 1, which features an AB-type block copolymer, a micellar structure forms in an aqueous medium if one segment of the block copolymer can provide interchain cohesive interactions sufficient for the micelle formation. Most drug carrier applications have been studied with AB- or ABA-type block copolymers because the close relationship between micelles' properties and the structure of polymers can be evaluated more easily with AB- or ABA-type block copolymers than with the other types of copolymers.

I describe two fundamental physicochemical characteristics of polymeric micelles in this section, and in the Passive drug targeting of solid tumors section, I describe the other beneficial drug-carrier characteristics (1.2). The first physico-chemical characteristic is the polymeric micelle's very small size as summarized in Table 1. Polymeric micelles are formed typically in a diameter range from 10 nm to 100 nm with a substantial narrow distribution. As described in Section 2, this size range is considered ideal for the attainment of stable, long-term circulation of the carrier system in the bloodstream. Alternatively, the small size of polymeric micelles is a big benefit in the sterilization processes in pharmaceutical productions. Polymeric micelles are easily (without micron-sized particle'sclogging) and inexpensively (without another separation process) sterilized by filtration using typical sterilization filters with 0.45-mm or 0.22-mm pores owing to a fact that polymeric micelles are essentially free of micro-sized particle's contamination. This is a good contrast to other typical pharmaceutical nano-sized carrier systems (e.g., nanoparticles, liposomes) which need a removal process of contaminated micron-sized particles.

The second physicochemical characteristic is high structural stability. It is known that polymeric micelles possess high structural stability provided by the entanglement of polymer chains in the inner core. This stability has two aspects: static and dynamic[10–13].

* Corresponding author. Medical Engineering Laboratory, Research Center for Medical Science, The Jikei University School of Medicine, 3-25-8, Nishi-shinbashi, Minato-ku, Tokyo 105-8461, Japan.
E-mail: <masajun2093ryo@jikei.ac.jp>

1878-3317/$ – see front matter
doi:10.1016/j.jecm.2011.06.002

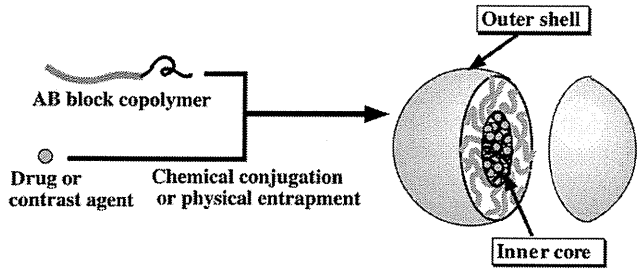

Figure 1 Design of a polymeric micelle carrier system.

Static stability is described by a critical micelle concentration (CMC). Generally, polymeric micelles show very low CMC values in a range from 1 μg/mL to 10 μg/mL. These values are much smaller than typical CMC values of micelles forming from low-molecular-weight surfactants. The second aspect, dynamic stability, is described by the low dissociation rates of micelles, and this aspect may be more important than the static one for *in vivo* drug delivery in physiological environments that are in nonequilibrium conditions. The high structural stability of polymeric micelles stated earlier is an important key to *in vivo* delivery in micellar forms and simultaneously eliminates the possible contribution of single polymer chains to drug delivery. Therefore, although they share the root word "micelle," polymeric micelles are very different from low-molecular-weight-surfactant micelles in their physicochemical properties. This difference is critical in the applications for drug carriers.

1.2. Advantages of polymeric micelle as a drug carrier

As summarized in Table 1, the third advantage of the polymeric micelle carrier system as a drug carrier is its high water solubility even when it incorporates a large amount of hydrophobic drugs[14]. Accordingly, "large amount of drug loading" is listed as the forth advantage. Generally, in conventional synthetic polymer-drug conjugate systems and antibody-drug conjugate systems, a loss of the carrier's water solubility resulting from the conjugation of a hydrophobic drug creates a serious problem. Several research groups reported this problem of the polymer-drug conjugates in syntheses[15–17] and in their intravenous injections[18]. Polymeric micelles can incorporate a large number of hydrophobic drug molecules in the micelles' inner core, and simultaneously, the micelles can maintain their water solubility by inhibiting intermicellar aggregation of the hydrophobic cores with a hydrophilic outer shell layer that works as a barrier against intermicellar aggregation. This is a great advantage because many potent drugs that have been developed in recent years are very hydrophobic and are, therefore, water insoluble.

The beneficial characteristic of low toxicity may be described as the fifth advantage. Generally, polymeric surfactants are known to be less toxic than low-molecular-weight surfactants, such as sodium dodecyl sulfate. Furthermore, in theory, polymeric micelles are considered very safe in relation to chronic toxicity. Possessing a much larger size than that for critical filtration in the kidney, polymeric micelles can evade renal filtration, even if the molecular weight of the constituting block copolymer is lower than the critical molecular weight for renal filtration. On the other hand, all polymer chains can be dissociated (as single polymer chains) from the micelles over a long time period. This phenomenon results in the complete excretion of the block copolymers from the renal route if the polymer chains are designed with a lower molecular weight than the critical value for renal filtration. Such a result constitutes an advantage of polymeric micelles over the conventional (non–micelle forming) and nonbiodegradable polymeric drug carrier systems.

The sixth advantage is the fact that various chemical species can be incorporated into polymeric micelles. As explained previously, the most commonly examined chemical species are hydrophobic low-molecular-weight organic compound drugs. These drugs can be incorporated into the micelle inner core either by chemical conjugation to the inner-core-forming polymer block or by physical entrapment owing to hydrophobic interactions between the entrapped drug molecules and the hydrophobic inner-core-forming polymer block. Hydrophobic interactions also work as a driving force for micelle formation. On the other hand, polymeric micelles are formed through ionic interactions between charged polymer chains. For example, polymeric micelles form from poly(ethylene glycol) (PEG)-b-poly(lysine) block copolymers and poly(aspartic acid) (ASP) homopolymers where the poly(lysine) chain is positively charged and the poly(ASP) chain is negatively charged. If negatively charged polypeptides[19] or nucleic acid[20] are used in place of poly(ASP), these pharmacologically active macromolecules are incorporated into polymeric micelles for protein, gene, and small interfering RNA delivery purposes. Furthermore, metal ions or metal ions' chelates can be incorporated into polymeric micelles through coordination bonds or ionic interactions. A platinum chelate cisplatin, which is a widely used anticancer drug, was successfully incorporated into polymeric micelles forming from PEG-b-poly(ASP) through a ligand exchange reaction between a carboxylic acid residue of the poly(ASP) chain and a chloride ion of cisplatin. [21–23] Alternatively, gadolinium (Gd) ions, which can work as a magnetic resonance imaging (MRI) contrast agent, were incorporated into polymeric micelles by the use of a chelate-moiety-conjugated block copolymer. [24–26] As stated above, various pharmaceutical drugs, genes, and contrast agents can be incorporated into polymeric micelles with appropriate choices of block copolymer structures.

1.3. Disadvantages of polymeric micelle as a drug carrier

It is worthwhile to explain the disadvantages of the polymeric micelle systems and the advantages described above. The four disadvantages are summarized in Table 2. Two of them are polymeric micelle-specific ones, whereas the other two disadvantages are common for polymeric carriers including non-micelle-forming systems. The first disadvantage is a fact that relatively high levels of polymer chemistry are needed in the polymeric micelle studies. As illustrated in Figure 1, an AB type of block copolymer is one of the most favorable structures for polymeric micelle carriers. The architecture of the AB block copolymer is very simple, however, its synthesis is more difficult than that of random polymers, where different units are aligned on a polymer chain in a random manner.

Table 1 Advantages of polymeric micelles as drug carriers

1. Very small size (diameter = 10–100 nm)
2. High structural stability
3. Large amount of drug loading
4. High water solubility
5. Low toxicity
6. Incorporation of various chemical species

Table 2 Disadvantages of polymeric micelle drug carriers

1. Specific disadvantages of polymeric micelle carriers
   - A. Difficult polymer synthesis
   - B. Immature drug-incorporation technology
2. Common disadvantages of polymeric carriers
   - A. Slow extravasation
   - B. Possible chronic liver toxicity due to slow metabolic process

Furthermore, researchers may encounter a problem in a synthesis of the block copolymer of a large industrial scale in a highly reproducible manner.

The second disadvantage, specifically, for the polymeric micelle systems is the immature technology for drug incorporation in a physical manner. Yokoyama et al reported that physical-incorporation efficiencies were dependent on various factors in drug-incorporation processes. Presently, there seem to be no universal incorporation method applicable to any polymer. Furthermore, in some methods the drug incorporation may be difficult on a large industrial scale, whereas the drug incorporation is easy and efficient on a small laboratory scale.

The third disadvantage (B-1 in Table 2) is much slower extravazation of polymeric carrier systems than that of low-molecular-weight drugs. This results from a difference in extravazation mechanisms between polymeric carrier systems and low-molecular-weight drugs. The polymeric systems translocate from the bloodstream to the interstitial space of organs and tissues through intra-cellular channels and inter-cellular junctions, whereas the drugs permeate directly through lipid bilayer cell membranes. Therefore, a long circulation character of the polymeric systems is an essential requirement for delivery of a therapeutic amount owing to compensation of the slow extravazation with a large Area Under the Curve value that results from the long circulation. The forth disadvantage is a risk of chronic liver toxicity. Drugs conjugated or incorporated in the polymeric carrier systems are metabolized in liver in a slower manner than free drug, since access of metabolic enzymes to drugs is inhibited because of the conjugation and incorporation. Therefore, toxic side effects of the conjugated and incorporated drug may be exhibited for a longer period than a case of free drug whose toxic effects can be lowered through metabolism in a short period.

2. Passive Drug Targeting to Solid Tumors

2.1. Methodology and significance of passive targeting to solid tumors

Drug targeting is defined as selective drug delivery to specific physiological sites—organs, tissues, or cells—where the drug's pharmacological activities are required. Different drug-targeting efforts could be thought of as reflecting one of two methods: active targeting and passive targeting[27,28]. Active targeting aims at an increase in the delivery of drugs to the target by using biologically specific interactions, such as antigen–antibody binding or by utilizing locally applied signals, such as heating and sonication. Carriers classified in this method include specific antibodies, transferrin, and thermoresponsive liposomes and polymeric micelles. On the other hand, passive targeting is defined as a method whereby the physical and chemical properties of carrier systems increase the target/nontarget ratio of a quantity of a delivered drug. Here, I discuss only passive drug targeting of solid tumors because the passive tumor-targeting method is important also for active tumor targeting. The reasons for this importance are twofold:

1. A greater part of a living body consists of nontarget sites. Even if a tumor occupies 1% of an entire body's weight (this would involve a very big tumor), the nontarget sites account for 99% of the body's weight (which is by no measure negligible, obviously). Drug carrier systems cannot access a target site once they are captured by nontarget sites. Therefore, the minimization of nonspecific capture at nontarget sites is important for active tumor targeting, and minimization is achieved in passive targeting.
2. Passive transfer phenomena precede biologically specific interactions for most active targeting systems (exceptions are cases of intravascular targets, such as vascular endothelial cells). Most tumor targets are located in extravascular space. To reach these targets through the bloodstream, the first step must be translocation through the vascular endothelium, followed by diffusion in the interstitial space. Even for active targeting systems based on cells' biologically specific receptors, such as tumor-specific antigens, the passive transendothelial step is both a necessary and an anterior one.

The passive targeting of polymeric micelles on solid tumors can be achieved owing to the enhanced permeability and retention effect (EPR effect). Maeda and Matsumura presented this passive drug-targeting strategy in 1986.[29–31] Vascular permeability of tumor tissues is enhanced by the actions of secreted factors, such as kinin and vascular permeability factor. As a result of this increased vascular permeability, macromolecules selectively increase their transport from blood vessels to tumor tissues. Furthermore, the lymphatic drainage system does not operate effectively in tumor tissues. Therefore, macromolecules are selectively retained for a prolonged time in the tumor interstitium. The EPR effect was first proven for a natural peptide, albumin, as shown in Figure 2. Evans blue-stained albumin was observed to accumulate at an S-180 tumor transplanted on skin in a much higher concentration than that which characterizes normal skin. The high concentrations at the tumor were maintained for a long period (upto 6 days) after intravenous injection. It is worth mentioning that a relatively long period is required (48 hours in Figure 2) for albumin to reach a peak concentration because macromolecular albumin has a much lower transvascular rate than is the case with low-molecular-weight drugs that reach the peak concentrations at tumors in a range between several minutes and several tens of minutes. After the discovery of the EPR effect for albumin, it was revealed that the EPR effect can also be applied to synthetic polymers and nano-sized carrier systems, such as liposomes and polymeric micelles. In the EPR effect, specific targeting moieties, such as antibodies are not necessary. However, the carrier systems must fulfill the following two requirements to avoid nonspecific capture at non-tumor sites:

1. The drug carrier systems must possess an appropriate size or molecular weight. The diameter of carriers must be smaller

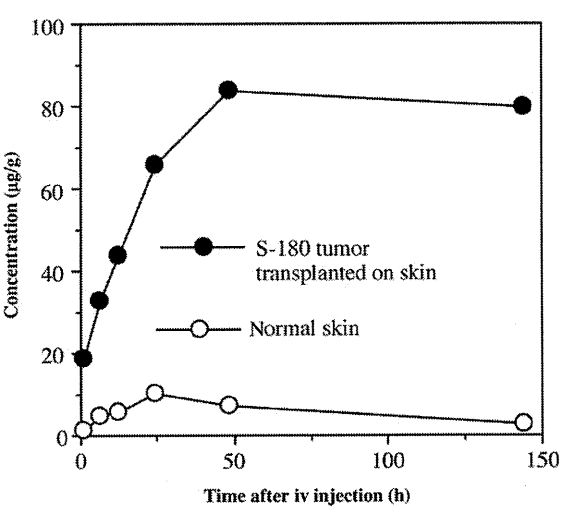

Figure 2 Enhanced permeability and retention effect shown with Evans blue-albumin. iv = intravenous.

than approximately 200 nm if the reticuloendothelial system's uptake is to be evaded.[32] Additionally, molecular weights greater than a critical value (approximately 40,000) are favorable for evading renal filtration.

2. The drug carrier systems must not exhibit strong interactions or uptake with or by normal organs (especially the reticuloendothelial systems). These strong interactions and uptakes are typically seen for cationic[33] and hydrophobic carriers.[34] Therefore, the carrier systems must possess hydrophilic surfaces, and their surface charge must be neutral or weakly negative. Furthermore, the carrier systems must possess no other chemical structures that would be biologically recognizable to normal tissues.

Concerning the two aforementioned requirements, polymeric micelles are very advantageous because polymeric micelles are formed in a diameter ranging from 10 nm to 100 nm. The size requirement for the EPR effect is inherently fulfilled for polymeric micelle drug carrier systems. Additionally, the second requirement can be easily fulfilled through a choice of hydrophilic and neutrally or weakly negatively charged polymers for the outer shell–forming block. With this choice, polymeric micelles can circulate in the bloodstream for a long time period by evading nonspecific capture, resulting in successful attainment of the EPR effect. Because most anticancer drugs are hydrophobic [and because a considerable number of anticancer drugs are positively charged molecules, such as doxorubicin (DOX)], inhibition of strong nonspecific interactions resulting from drug molecules is a critical matter for the attainment of the EPR effect. For efficient EPR-effect-attainment, polymeric micelle carrier systems have a great advantage in their phase-separated structure, in which the drug-incorporating inner core is structurally separated from the outer shell that plays an essential role in interactions with the nontarget normal organs.

2.2. *An example of polymeric micelle's passive tumor targeting*

Here, I introduce the first successful example of tumor targeting with a polymeric micelle carrier. Yokoyama, Okano, and Kataoka et al succeeded in getting an anticancer drug, doxorubicin (DOX) (=adriamycin), with a polymeric micelle system, to passively target solid tumors[35–45] was chemically conjugated to ASP residues of PEG-poly(ASP) block copolymers (PEG-poly(Asp)) by amide bond formation. The PEG segment was hydrophilic, whereas the DOX-conjugated poly(ASP) chain was hydrophobic. Therefore, the obtained drug-block copolymer conjugate (PEG-poly(Asp(DOX))) formed micellar structures owing to its amphiphilic character. In the second step, DOX was incorporated into the inner core by physical entrapment using hydrophobic interactions with the chemically conjugated DOX molecules. As a result, polymeric micelles containing both the chemically conjugated and the physically entrapped DOX in the inner core were obtained with the PEG outer shell. It was revealed that only physically entrapped DOX exerted anticancer activity, and that the chemically conjugated DOX did not show any cytotoxic activity.

The physically entrapped DOX circulated in the bloodstream for a long time and was delivered to the solid tumor site at much higher concentrations than that of free DOX as shown in Figure 3.[39] Furthermore, the observed time profile with a peak concentration at 24 hours post–intravenous injection and postinjection retention of these high concentrations for longer time periods were highly consistent with passive delivery by the EPR effect[29] as shown in Figure 2 for albumin. On the other hand, accumulation of the physically entrapped DOX in the polymeric micelles in normal organs and tissues was the same as or lower than the accumulation of free DOX. As a result of the aforementioned biodistributions, high

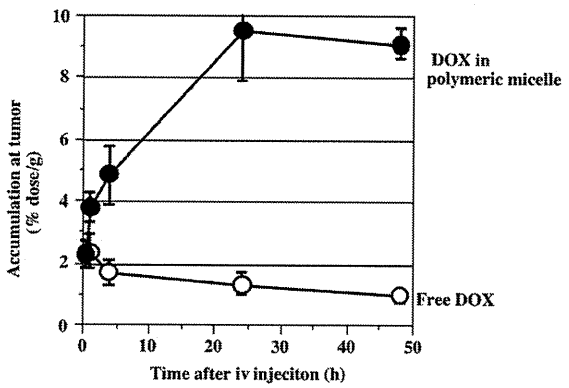

Figure 3 Passive targeting of a DOX-containing polymeric micelle. DOX = doxorubicin; iv = intravenous.

ratios of tumor to normal organs or of tumor to normal tissues were successfully obtained, as summarized in Table 3. In accordance with this highly selective delivery to solid tumor sites, dramatic enhancement of antitumor activity was observed.[39] Complete tumor eradication against murine colon adenocarcinoma 26 (C26) was achieved at two doses of DOX-incorporated polymeric micelles, whereas partial inhibition of tumor growth was obtained only at one maximum tolerated dose for free DOX. All these results clearly demonstrate the successful passive targeting of a solid tumor by an anticancer drug with the polymeric micelle carrier system.

I would like to make two additional comments on this DOX-incorporated polymeric micelle. First, concerning selectivity, a considerably high tumor to heart ratio was obtained in measurements with radiolabel on the physically entrapped DOX, as summarized in Table 2. From clinical viewpoints, this is very important because cardiotoxicity is a critical toxicity of DOX. Therefore, this high ratio suggests that the system has high clinical potential although the cardiotoxicity was not evaluated in this *in vivo* study. However, this ratio value does not suggest a specific limit to the targeting selectivity in the EPR effect–based passive targeting because no detectable amount was found in the heart when biodistribution was measured with radiolabeled chemically conjugated DOX. This fact indicates a route of delivery to the heart of the physically entrapped DOX; the physically entrapped DOX was released from the polymeric micelle in the bloodstream, and the released DOX accumulated at the heart. Therefore, a higher tumor to heart selective ratio can be obtained through further optimization of the DOX drug-release rate.

The second point concerns accumulation behavior at the liver. The report by Yokoyama et al[39] identifies an interesting pharmacokinetic behavior of the micellar DOX. Within 1 hour after intravenous injection, an accumulated amount of the micellar DOX in the liver was smaller than that of free DOX. This inequality indicates that the targeting strategy based on the EPR effect was effective in this targeting system even for the liver, which is known to possess pores large enough for micelles' extravasation in the liver's vasculature. In contrast, at 4 hours and later, after intravenous injection,

Table 3 Tumor-targeting selectivity of DOX-incorporated polymeric micelle (24 hours after intravenous injection)

	Accumulated amount at tumor (% dose/g tumor)	Ratio of accumulated amounts	
		Tumor:heart	Tumor:muscle
DOX-incorporated polymeric micelle	9.6	5.8	11.5
Free DOX	1.1	1.3	1.2

DOX = doxorubicin.

this situation was reversed. The micellar DOX exhibited larger accumulation amounts in the liver than free DOX. This inequality resulted from rapid clearance of free DOX in the liver through the liver's metabolic activity for drugs, whereas the micellar DOX concentration in the liver did not undergo a significant drop, probably because the physically entrapped DOX in the micelle core was greatly protected from the metabolic activity. Consequently, the concentration of the micellar DOX was several-fold larger than that of the free DOX. However, toxic side effects of the DOX polymeric micelle system in the liver was on the same level of the free DOX as observed in alanine aminotransferase- and aspartate transaminase-level measurements. This means that the liver toxicity was not enhanced in the DOX polymeric micelle. Therefore, chronic liver toxicity merits careful examination not only for the polymeric micelle systems but also for all nano-sized drug carrier systems, such as PEG-coated liposomes, particularly for drugs for which liver toxicity is a major adverse effect.

3. Contrast Agent Targeting[24–26,40–47]

As described in the Passive drug targeting of solid tumors section, drug molecules were successfully targeted at solid tumors by the use of polymeric micelle carriers. It is a natural way to expand this tumor-targeting application of contrast agents. If contrast agents are targeted at solid tumors, clearer tumor images can be obtained with contrast agent carrier systems[24–26,41,42,44,45,47] than conventional image diagnosis of tumors. The targeted contrast agents not only provide high contrast in tumor images but also can lower the size limit of small tumor detection. In the present diagnoses of tumors, it is not easy to detect tumors whose size is less than 1 cm in diameter in the image diagnosis, and therefore, the ability to detect tumors smaller than 1 cm in diameter is considered a big success of imaging diagnosis. On the other hand, the minimum size attributable to tumors expressing the EPR effect is considered to be approximately 2–3 mm in diameter for the following two reasons.[31]

First, the enhanced permeability of tumor vasculatures is considered to be one physiological phenomenon of angiogenesis.[48–50] Two, tumors are expected to start exhibiting angiogenesis at approximately 2–3 mm in diameter because tumors encounter a serious problem in oxygen supply from the normal blood vessels beyond this tumor size.[51–53] Angiogenesis is a phenomenon involving sufficient oxygen supply to tumor cells from newly formed blood vessels in the tumor tissue. This minimum size should be dependent on tumor type and species. Although there are no solid data concerning the minimum tumor size for the EPR effect's expression, many articles have reported EPR effect–based tumor targeting for tumors of approximately 5–6 mm in diameter.[34,35,54,55] In targeting chemotherapy, efficacy against large tumors is meaningful. In contrast, in the targeting contrast agent case, successful targeting of smaller tumors is more highly appreciated because the success leads to the detection of small tumors—a type of detection that is of much value but is often scarce in present cancer medicine. As stated earlier, contrast agents exhibiting EPR effect–based tumor targeting may greatly contribute in reducing the minimum size of tumor detection in clinic.

In addition to the aforementioned clinical significance of the EPR effect–based tumor-targeting contrast agents, a clinical merit results from a combination of image diagnosis and chemotherapy by the use of a single carrier system. The concept of this combination medicine is illustrated in Figure 4. In human clinical cases, tumor characteristics (e.g., growth rate, metastatic activity, angiogenesis, tumor blood vessel density, vascular permeability) vary among each patient to a much greater degree than in animal tumor models, which tend toward uniformity regarding these

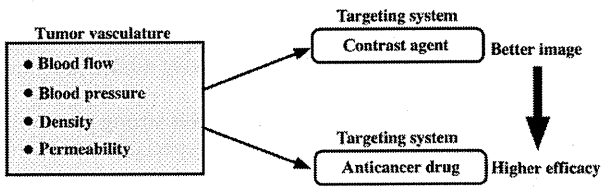

Figure 4 Combination of image diagnosis and chemotherapy against a tumor by means of a single carrier system.

characteristics. For EPR-based targeting of solid tumors, the following four characteristics are considered important: degree of blood flow, blood pressure, density, and permeability (for nano-sized carriers) of tumor vasculature. If one patient's tumor exhibits favorable aspects in these characteristics (high blood flow, high blood pressure, high density, and high permeability), this tumor is expected to provide a clear image in an image diagnosis if an EPR effect–based contrast agent is used for visualization of the tumor. Accordingly, considerable antitumor activity is also expected against this well-visualized tumor when targeted chemotherapy is performed on this patient with the same carrier system incorporating anticancer drugs. Therefore, this combined medical system can provide a greater response rate for the patients whose tumors are clearly visualized in the imaging diagnosis with the nano-sized contrast agent system. As described in the Section 1.2, polymeric micelle carrier systems possess a great advantage in terms of ability to incorporate various kinds of chemical species, contrast agents, and anticancer drugs. Therefore, polymeric micelles are favorable as a carrier for combined diagnosis and therapy systems.

To obtain the combined (dual) targeting system described earlier, Shiraishi and Yokoyama et al[24–26] reported a polymeric micelle MRI contrast agent. Using a poly(ethylene glycol)-b-poly(L-lysine) block copolymer derivative[25], they prepared a polymeric micelle binding Gd ions that enhance MRI contrasts by shortening the T_1 relaxation times of protons of water. This polymeric micelle was found to be targeted to a murine tumor C26, and the tumor was successfully visualized with the targeted MRI contrast agent. It is worth mentioning that biodistribution of the MRI contrast agent was the same as that of an anticancer drug-targeting system. As shown in Figure 5, distributions of the Gd-ion-containing polymeric micelle in a C26 murine solid tumor, the heart, and muscle were the same as with those of a DOX-containing polymeric micelle. This fact indicates the feasibility of the combined tumor medicine of MRI image diagnosis and chemotherapy by the use of the polymeric micelle carrier system that carries an MRI contrast agent and an anticancer drug.

4. Future Perspectives

Currently (January 2011), Japanese, US, and British teams are examining clinical trials for five polymeric micelle anticancer drug-targeting systems, as summarized in Table 4 [Additional two polymeric micelle formulations (No. 6 and 7) whose purpose is other than targeting have also been listed].[56–72] Chemical structures of the inner-core-forming polymer blocks vary depending on the incorporated drug, whereas the PEG chain is used for the outer shell in all cases. Tumor targeting is the primary objective of these carrier systems. However, these systems possess another objective: the system exhibits a function to solubilize a water-insoluble drug. Matsumura et al reported that NK-105-incorporating paclitaxel exhibited highly tumor-selective delivery in murine tumor models.[60,62,63] In clinical stages, NK-105 can

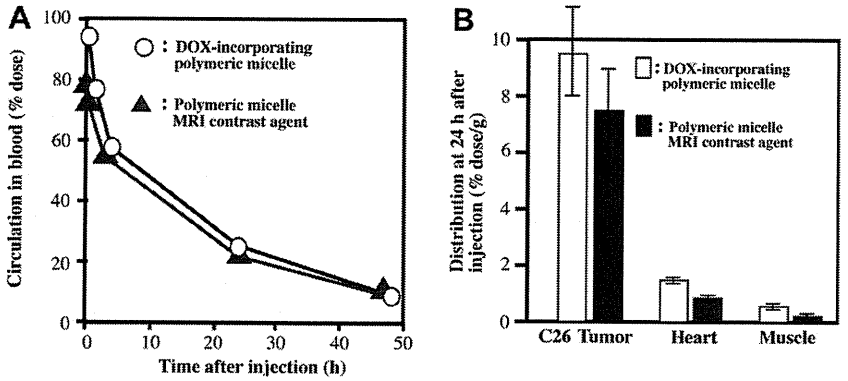

Figure 5 Comparisons of the biodistribution of two polymeric micelles. (A) Blood and (B) tumor, heart, and muscle. DOX = doxorubicin; MRI = magnetic resonance imaging.

exhibit two solubilization-related advantages over the conventional paclitaxel formulation Taxol (Bristol-Myers Squibb, Priceton, NJ, USA). The first advantage attributable to NK-105 is its relatively low toxic side effects, which reflects the fact that the block copolymer is much less toxic than Cremophor EL used in Taxol. The second advantage attributable to NK-105 is that it does not need the premedication that Taxol requires for reducing its own side effects.

We must wait for the final results of clinical trials to answer the question "Are the polymeric micelle systems effective and approved in cancer chemotherapy?" While waiting for the answer, we can take comfort in the fact that Phase I clinical studies have already yielded important information concerning toxic side effects.[56–60] Even for targeted drugs, serious side effects arise because doses are escalated until dose-limiting toxicities become observable. The important obtained information has revealed the toxicity profiles of the polymeric micelle drugs, which turned out to be the same as those of the corresponding free drugs. Most of the toxic side effects of the polymeric micelle drugs appear to result from the carriers' release of the drug in the bloodstream. The absence of uncommon and unexpected types of toxicities is a greatly meaningful fact that can contribute to the safety of clinical use. We have not obtained enough clinical results to draw a general conclusion that synthetic block copolymers can be safely used in clinical stages. However, basic-study researchers and clinicians must develop their studies while keeping in mind this potential clinical advantage of the drug carrier.

Here, I would like to describe future perspectives on polymeric micelle research and developments in cancer treatment. First, various combinations of anticancer drugs and cancers should and will be examined. In the anticancer drug–incorporated polymeric micelle systems listed in Table 4, choices of anticancer drugs have been made according to the general usefulness and effectiveness of the drugs in cancer chemotherapy. In the future, polymeric micelle anticancer drugs can be studied with regard to the different reasons for the anticancer drugs' general usefulness. One example is the use of retinoids. Retinoids, such as *cis*-retinoic acid, express their anticancer activity through differentiation of cancer cells, not through cytotoxic actions that are common in most currently available anticancer drugs. We successfully incorporated *cis*-retinoic acid and other retinoids into polymeric micelle carriers.[70–74] If we compared these *in vivo* anticancer activities with those of the polymeric micelles containing common cytotoxic anticancer drugs, we would see that the retinoid-incorporated polymeric micelles would exhibit lower levels of activity than the cytotoxic ones. However, I believe, owing to the unique action mechanism of the retinoids, retinoid-incorporated polymeric micelles may exhibit great therapeutic effects against specific cancers. Alternatively, polymeric micelle systems may be used in an injection route other than the intravenous route. One example is convection-enhanced delivery to brain tumors. This is a direct injection to brain solid tumors with a special injection needle and a very slow rate of injection, such as 5 μL/min. In a special corresponding application, polymeric micelle carriers were used for inhibition of rapid elimination from the injection site through the bloodstream.[74,75] If small-molecular-weight anticancer drugs are injected by the convection-enhanced delivery, they are very rapidly eliminated from the injection site owing to their high translocation rates through vascular endothelia. Accordingly, effective anticancer activity cannot be obtained. This is a novel application approach to polymeric micelle systems.

My second perspective concerns the combination of anticancer drug targeting and contrast agent targeting as described in the previous section. Visualization of small tumors with the EPR effect–based targeting contrast agents is one example of molecular targeting because the hyperpermeability of tumor vasculature is a physiological event induced by angiogenesis-related molecules, such as the vascular permeability factor and kinin. Molecular imaging is one hot and rapidly developing field in the 21st century. Therefore, clinical developments in drug-targeting therapy can be accelerated if drug targeting is combined with molecular imaging.

The third perspective concerns a combined use of a drug that boosts the EPR effect. The hyperpermeability of tumor vasculature essential for the EPR effect is induced by natural factors originating in tumor cells. Recently, artificial induction and escalation of the hyperpermeability have been examined for enhancement of EPR effect–based tumor targeting. Transforming growth factor-β inhibitors,[76,77] nitroglycerin,[78] and a combretastatin derivative[79] have been examined for tumor-targeting enhancements of macromolecular drugs or polymeric micelles. In particular, nitroglycerin is an approved drug for angina pectoris, and the combretastatin derivative known as cderiv is an anti-cancer drug under clinical trial (the combretastatin derivative known as cderiv); therefore, their clinical applications are feasible. All these studies are in a basic stage with animal experiments. I believe that once

Table 4 Polymeric micelle anticancer drug-targeting systems in clinical trials

No.	Trade name	Purpose	Incorporated drug	Progress	References*
1	NK-911	Targeting	Doxorubicin	Phase II	46
2	NK-105	Targeting	Paclitaxel	Phase II	47, 49, 50
3	NK-012	Targeting	SN-38	Phase II	52
4	NC-6004	Targeting	Cisplatin	Phase I	21, 48
5	NC-4016	Targeting	DACH-platin	Phase I	51
6	Genexol-PM	Solubilization	Paclitaxel	Approved	63, 64
7	SP-1049C	Anti-MDR effect	Doxorubicin	Phase II	65, 66

* Review references 56–58 cover No. 1–5 systems.

authorities approve a polymeric micelle anticancer drug product, its applications will likely undergo dramatic expansion owing to the use of these hyperpermeablity-inducing agents.

References

1. Aliabadi M, Lavasanifar A. Polymeric micelles for drug delivery. *Expert Opin Drug Deliv* 2006;**3**:139–62.
2. Adams ML, Lavasanifar A, Kwon GS. Amphiphilic block copolymers for drug delivery. *J Pharm Sci* 2003;**92**:1343–55.
3. Yokoyama M. Block Copolymers as drug Carriers. *Crit Rev Ther Drug Carrier Syst* 1992;**9**:213–48.
4. Yokoyama M. Polymeric micelles for the targeting of hydrophobic drugs. In: Kwon GS, editor. *Drug and pharmaceutical sciences vol. 148 polymeric drug delivery systems.* Boca Raton: Taylor & Francis; 2005. p. 533–75.
5. Yokoyama M. Polymeric micelles as nano-sized drug carrier systems. In: Tabata Y, editor. *Nanoparticles for pharmaceutical applications.* Stevenson Ranch: American Scientific Publishers; 2007. p. 63–72.
6. Yokoyama M. Polymeric micelles as a novel drug carrier system and their required considerations for clinical trials. *Expert Opin Drug Deliv* 2010;**7**: 145–58.
7. Kedar U, Phutane P, Shidhaye S, Kadam V. Advances in polymeric micelles for drug delivery and tumor targeting. *Nanomedicine* 2010;**6**:714–29.
8. Oerlemans C, Bult W, Bos M, Storm G, Nijsen JF, Hennink WE. Polymeric micelles in anticancer therapy: targeting, imaging and triggered release. *Pharm Res* 2010;**27**:2569–89.
9. Tuzar Z, Kratochvil P. Block and graft copolymer micelles in solution. *Adv Colloid Interface Sci* 1976;**6**:201–32.
10. Calderara F, Hruska Z, Hurtrez G, Lerch JP, Nugay T, Riess G. Investigation of polystyrene-poly(ethylene oxide) block copolymer micelle formation in organic and aqueous solutions by nonradiative energy transfer experiments. *Macromolecules* 1994;**27**:1210–5.
11. Wang Y, Kausch CM, Chun M, Quirk RP, Mattice WL. Exchange of chains between micelles of labeled polystyrene-block-poly(oxyethylene) as monitored by nonradiative singlet energy transfer. *Macromolecules* 1995;**28**:904–11.
12. Wilhelm M, Zhao CL, Wang Y, Xu R, Winnik RA. Poly(styrene-ethylene oxide) block copolymer micelle formation in water: a fluorescence probe study. *Macromolecules* 1991;**24**:1033–40.
13. Desjardins A, Eisenberg A. Colloidal properties of block ionomers. I. Characterization of reverse micelles of styrene-b-metal methacrylate diblocks by size-exclusion chromatography. *Macromolecules* 1991;**24**:5779–90.
14. Yokoyama M, Kwon GS, Kataoka K. Preparation of micelle-forming polymer-drug conjugates. *Bioconjugate Chem* 1992;**3**:295–301.
15. Hoes CJT, Potman W, Feijen J. Optimization of macromolecular prodrugs of the antitumor antibiotic adriamycin. *J Control Release* 1985;**2**:205–13.
16. Duncan R, Kopeckova-Rejmanova P, Kopecek J. Anticancer agents coupled to N-(2-hydroxypropyl)methacrylamide copolymers I. Evaluation of daunomycin and puromycin conjugates *in vitro*. *Br J Cancer* 1987;**55**:165–74.
17. Endo N, Umemoto N, Hara T. A novel covalent modification of antibodies at their amino groups with retention of antigen-binding activity. *J Immunol Methods* 1987;**104**:253–8.
18. Zunino F, Pratesi G, Micheloni A. Poly(carboxylic acid) polymers as carriers for anthracyclines. *J Control Release* 1989;**10**:65–73.
19. Harada A, Kataoka K. Novel polyion complex micelles entrapping enzyme molecules in the core: Preparation of narrowly-distributed micelles from lysozyme and poly(ethylene glycol)-poly(aspartic acid) block copolymer in aqueous medium. *Macromolecules* 1998;**31**:288–94.
20. Kataoka K, Togawa H, Harada A, Yasugi K, Matsumoto T, Katayose S. Spontaneous formation of polyion complex micelles with narrow distribution from antisense oligonucleotide and cationic block copolymer in physiological saline. *Macromolecules* 1996;**29**:8556–7.
21. Yokoyama M, Okano T, Sakurai Y, Suwa S, Kataoka K. Introduction of cisplatin into polymeric micelle. *J Control Release* 1996;**39**:351–6.
22. Nishiyama N, Yokoyama M, Aoyagi T, Okano T, Sakurai Y, Kataoka K. Preparation and characterization of self-assembled polymer-metal complex micelle from cis-dichlorodiammineplatinum (II) and poly(ethylene glycol)-poly(α,β-aspartic acid) block copolymer in an aqueous medium. *Langmuir* 1999;**15**:377–83.
23. Nishiyama N, Okazaki S, Cabral H, Miyamoto M, Kato Y, Sugiyama Y, Nishio K, et al. Novel cisplatin-incorporated polymeric micelles can eradicate solid tumors in mice. *Cancer Res* 2003;**63**:8977–83.
24. Nakamura E, Makino K, Okano T, Yamamoto T, Yokoyama M. A polymeric micelle MRI contrast agent with changeable relaxivity. *J Control Release* 2006;**114**:325–33.
25. Shiraishi K, Kawano K, Minowa T, Maitani Y, Yokoyama M. Preparation and in vivo imaging of PEG-poly(L-lysine)-based polymeric micelle MRI contrast agents. *J Control Release* 2009;**136**:14–20.
26. Shiraishi K, Kawano K, Maitani Y, Yokoyama M. Synthesis of poly(ethylene glycol)-b-poly(L-lysine) block copolymers having Gd-DOTA as MRI contrast agent and their polymeric micelle formation by polyion complexation. *J Control Release* 2010;**148**:160–7.
27. Yokoyama M, Okano T. Targetable drug carriers: Present status and a future perspective. *Adv Drug Deliv Rev* 1996;**21**:77–80.
28. Sugiyama Y. Importance of pharmacokinetic considerations in the development of drug delivery systems. *Adv Drug Deliv Rev* 1996;**19**:333–4.
29. Matsumura Y, Maeda H. A new concept for macromolecular therapeutics in cancer chemotherapy: Mechanism of tumoritropic accumulation of proteins and the antitumor agent smancs. *Cancer Res* 1986;**46**:6387–92.
30. Maeda H, Seymour LW, Miyamoto Y. Conjugates of anticancer agents and polymers: advantages of macromolecular therapeutics *in vivo*. *Bioconjug Chem* 1992;**3**:351–61.
31. Fang J, Nakamura H, Maeda H. The EPR effect: Unique features of tumor blood vessels for drug delivery, factors involved, and limitations and augmentation of the effect. *Adv Drug Deliv Rev* 2011;**63**:136–51.
32. Litzinger DC, Buiting AMJ, van Rooijen N, Huang L. Effect of liposome size on the circulation time and intraorgan distribution of amphipathic poly(ethylene glycol)-containing liposomes. *Biochim Biophys Acta* 1994;**1190**:99–107.
33. Takakura Y, Hashida M. Macromolecular carrier systems for targeted drug delivery: Pharmacokinetic consideration on biodistribution. *Pharm Res* 1996; **13**:820–31.
34. Illum L, Davis SS, Miller RH, Mak E, West P. The organ distribution and circulation time of intravenously injected colloidal carriers sterically stabilized with a block copolymer – Poloxamine 908. *Life Sci* 1987;**40**:367–74.
35. Yokoyama M, Inoue S, Kataoka K, Yui N, Sakurai Y. Preparation of adriamycin-conjugated poly(ethylene glycol)-poly(aspartic acid) block copolymer. A new type of polymeric anticancer agent. *Makromolekulare Chemie Rapid Communications* 1987;**8**:431–5.
36. Yokoyama M, Miyauchi M, Yamada N, Okano T, Sakurai Y, Kataoka K, Inoue S. Characterization and anti-cancer activity of micelle-forming polymeric anticancer drug, adriamycin-conjugated poly(ethylene glycol)-poly(aspartic acid) block copolymer. *Cancer Res* 1990;**50**:1693–700.
37. Yokoyama M, Okano T, Sakurai Y, Ekimoto H, Shibazaki C, Kataoka K. Toxicity and antitumor activity against solid tumors of micelle-forming polymeric drug and its extremely long circulation in blood. *Cancer Res* 1991;**51**: 3229–36.
38. Kwon GS, Suwa S, Yokoyama M, Okano T, Sakurai Y, Kataoka K. Enhanced tumor accumulation and prolonged circulation times of micelle-forming poly(ethylene oxide-aspartate) block copolymer-adriamycin conjugates. *J Control Release* 1994;**29**:17–23.
39. Yokoyama M, Okano T, Sakurai Y, Fukushima S, Okamoto K, Kataoka K. Selective delivery of adriamycin to a solid tumor using a polymeric micelle carrier system. *J Drug Target* 1999;**7**:171–86.
40. Lammers T, Kiessling F, Hennink WE, Storm G. Nanotheranostics and image-guided drug delivery: current concepts and future directions. *Mol Pharm* 2010;**7**:1899–912.
41. Lu ZR, Ye F, Vaidya A. Polymer platforms for drug delivery and biomedical imaging. *J Control Release* 2007;**122**:269–77.
42. Bogdanov Jr A, Wright SC, Marecos EM, Bogdanova A, Martin C, Petherick P, Weissleder R. A long-circulating co-polymer in "passive targeting" to solid tumors. *J Drug Target* 1997;**4**:321–30.
43. Gupta H, Weissleder R. Targeted contrast agents in MR imaging. *Magn Reson Imaging Clin N Am* 1996;**4**:171–84.
44. Bogdanov AA, Lewin M, Weissleder R. Approaches and agents for imaging the vascular system. *Adv Drug Deliv Rev* 1999;**37**:279–93.
45. Lebdusková P, Kotek J, Hermann P, Vander Elst L, Muller RN, Lukes I, Peters JA. A gadolinium(III) complex of a carboxylic-phosphorus acid derivative of diethylenetriamine covalently bound to inulin, a potential macromolecular MRI contrast agent. *Bioconjug Chem* 2004;**15**:881–9.
46. Caravan P, Ellison JJ, McMurry TJ, Lauffer RB. Gadolinium(III) chelates as MRI contrast agents: structure, dynamics, and applications. *Chem Rev* 1999;**99**: 2293–352.
47. Pathak AP, Gimi B, Glunde K, Ackerstaff E, Artemov D, Bhujwalla ZM. Molecular and functional imaging of cancer: advances in MRI and MRS. *Methods Enzymol* 2004;**386**:3–60.
48. Nagy JA, Benjamin L, Zeng H, Dvorak AM, Dvorak HF. Vascular permeability, vascular hyperpermeability and angiogenesis. *Angiogenesis* 2008;**11**: 109–19.
49. Dvorak HF, Nagy JA, Dvorak JT, Dvorak AM. Identification and characterization of the blood vessels of solid tumors that are leaky to circulating macromolecules. *Am J Pathol* 1988;**133**:95–109.
50. Dvorak HF, Brown LF, Detmar M, DvorakReview AM. Vascular permeability factor/vascular endothelial growth factor, microvascular hyperpermeability, and angiogenesis. *Am J Pathol* 1995;**146**:1029–39.
51. Folkman J, Shing Y. Angiogenesis. *J Biol Chem* 1992;**267**:10931–4.
52. Folkman J. Seminars in Medicine of the Beth Israel Hospital, Boston. Clinical applications of research on angiogenesis. *N Engl J Med* 1995;**333**:1757–63.
53. Holmgren L, O'Reilly MS, Folkman J. Dormancy of micrometastases: balanced proliferation and apoptosis in the presence of angiogenesis suppression. *Nat Med* 1995;**1**:149–53.
54. Ishida O, Maruyama K, Tanahashi H, Iwatsuru M, Sasaki K, Eriguchi M, Yanagie H. Liposomes bearing polyethyleneglycol-coupled transferrin with intracellular targeting property to the solid tumors *in vivo*. *Pharm Res* 2001;**18**: 1042–8.
55. Seymour LW, Miyamoto Y, Maeda H, Brereton M, Strohalm J, Ulbrich K, Duncan R. Influence of molecular weight on passive tumour accumulation of a soluble macromolecular drug carrier. *Eur J Cancer* 1995;**31A**:766–70.
56. Matsumura Y, Kataoka K. Preclinical and clinical studies of anticancer agent-incorporating polymer micelles. *Cancer Sci* 2009;**100**:572–9.

57. Matsumura Y. Polymeric micellar delivery systems in oncology. *Jpn J Clin Oncol* 2008;**38**:793–802.
58. Matsumura Y. Poly (amino acid) micelle nanocarriers in preclinical and clinical studies. *Adv Drug Deliv Rev* 2008;**60**:899–914.
59. Matsumura Y, Hamaguchi T, Ura T, Muro K, Yamada Y, Shimada Y, Shirao K, et al. Phase I clinical trial and pharmacokinetic evaluation of NK911, a micelle-encapsulated doxorubicin. *Br J Cancer* 2004;**91**:1775–81.
60. Hamaguchi T, Kato K, Yasui H, Morizane C, Ikeda M, Ueno H, Muro K, et al. A phase I and pharmacokinetic study of NK105, a paclitaxel-incorporating micellar nanoparticle formulation. *Br J Cancer* 2007;**97**:170–6.
61. Uchino H, Matsumura Y, Negishi T, Koizumi F, Hayashi T, Honda T, Nishiyama N, et al. Cisplatin-incorporating polymeric micelles (NC-6004) can reduce nephrotoxicity and neurotoxicity of cisplatin in rats. *Br J Cancer* 2005;**93**:678–87.
62. Negishi T, Koizumi F, Uchino H, Kuroda J, Kawaguchi T, Naito S, Matsumura Y. NK105, a paclitaxel-incorporating micellar nanoparticle, is a more potent radiosensitising agent compared to free paclitaxel. *Br J Cancer* 2006;**95**:601–6.
63. Hamaguchi T, Matsumura Y, Suzuki M, Shimizu K, Goda R, Nakamura I, Nakatomi I, et al. NK105, a paclitaxel-incorporating micellar nanoparticle formulation, can extend in vivo antitumour activity and reduce the neurotoxicity of paclitaxel. *Br J Cancer* 2005;**92**:1240–6.
64. Cabral H, Nishiyama N, Kataoka K. Optimization of (1,2-diamino-cyclohexane) platinum(II)-loaded polymeric micelles directed to improved tumor targeting and enhanced antitumor activity. *J Control Release* 2007;**121**:146–55.
65. Koizumi F, Kitagawa M, Negishi T, Onda T, Matsumoto S, Hamaguchi T, Matsumura Y. Novel SN-38-incorporating polymeric micelles, NK012, eradicate vascular endothelial growth factor-secreting bulky tumors. *Cancer Res* 2006; **66**:10048–56.
66. Kim DW, Kim SY, Heo DS, Kim HK, Kim SW, Shin SW, Kim JS, et al. Multicenter phase II trial of Genexol-PM, a novel Cremophor-free, polymeric micelle formulation of paclitaxel, with cisplatin in patients with advanced non-small-cell lung cancer. *Ann Oncol* 2007;**18**:2009–14.
67. Lee KS, Chung HC, Ro J, Im SA, Park YH, Kim CS, Kim SB, et al. Multicenter phase II trial of Genexol-PM, a Cremophor-free, polymeric micelle formulation of paclitaxel, in patients with metastatic breast cancer. *Breast Cancer Res Treat* 2008;**108**:241–50.
68. Sharma AK, Zhang L, Li S, Kelly DL, Alakhov VY, Batrakova EV, Kabanov AV, et al. Prevention of MDR development in leukemia cells by micelle-forming polymeric surfactant. *J Control Release* 2008;**131**:220–7.
69. Danson S, Alakhov V, Ranson M, Ferry D, Margison J, Kerr D, Jowle D, et al. Phase I dose escalation and pharmacokinetic study of pluronic polymer-bound doxorubicin (SP1049C) in patients with advanced cancer. *Br J Cancer* 2004; **90**:2085–91.
70. Chansri N, Kawakami S, Yokoyama M, Yamamoto T, Charoensit P, Hashida M. Anti-tumor effect of all-*trans* retinoic acid loaded polymeric micelles in solid tumor bearing mice. *Pharm Res* 2008;**25**:428–34.
71. Okuda T, Kawakami S, Yokoyama M, Yamamoto T, Yamashita F, Hashida M. Block copolymer design for stable encapsulation of N-(4-hydroxyphenyl) retinamide into polymeric micelles in mice. *Int J Pharm (Note)* 2008;**357**: 318–22.
72. Okuda T, Kawakami S, Higuchi Y, Satoh T, Oka Y, Yokoyama M, Yamashita F, et al. Enhanced in vivo antitumor efficacy of fenretinide encapsulated in polymeric micelles. *Int J Pharmaceutics* 2009;**373**:100–6.
73. Satoh T, Higuchi Y, Kawakami S, Hashida M, Kagechika H, Shudo K, Yokoyama M. Encapsulation of the synthetic retinoids Am80 and LE540 into polymeric micelles and the retinoids' release control. *J Control Release* 2009; **136**:187–95.
74. Yokosawa M, Sonoda Y, Sugiyama S, Saito R, Yamashita Y, Nishihara M, Satoh T, et al. Convection-enhanced delivery of a synthetic retinoid Am80, loaded into polymeric micelles, prolongs the survival of rats bearing intracranial glioblastoma xenografts. *Tohoku J Exp Med* 2010;**221**:257–64.
75. Inoue T, Yamashita Y, Nishihara M, Sugiyama S, Sonoda, Kumabe T, Yokoyama M, et al. Therapeutic efficacy of a polymeric micellar doxorubicin infused by convection-enhanced delivery against intracranial 9L brain tumor models. *Neuro-Oncology* 2009;**11**:151–7.
76. Kano MR, Bae Y, Iwata C, Morishita Y, Yashiro M, Oka M, Fujii T, et al. Improvement of cancer-targeting therapy, using nanocarriers for intractable solid tumors by inhibition of TGF-beta signaling. *Proc Natl Acad Sci USA* 2007;**104**:3460–5.
77. Minowa T, Kawano K, Kuribayashi H, Shiraishi K, Sugino T, Hattori Y, Yokoyama M, et al. Increase in tumor permeability following TGF-b type I receptor inhibitor treatment observed by dynamic contrast-enhanced MRI. *Br J Cancer* 2009;**101**:1884–90.
78. Seki T, Fang J, Maeda H. Enhanced delivery of macromolecular antitumor drugs to tumors by nitroglycerin application. *Cancer Sci* 2009;**100**:2426–30.
79. Hori K, Nishihara M, Yokoyama M. The combretastatin derivative cderiv, a vascular disrupting agent, enables polymeric nanomicelles to accumulate in microtumors. *J Pharm Sci* 2010;**99**:2914–25.

J Neurosurg Pediatrics 7:11–14, 2011

Surgical treatment and perioperative management of moyamoya disease associated with glycogen storage disease Type 1a

Case report

Yusuke Egashira, M.D.,[1] Jun C. Takahashi, M.D., Ph.D.,[1] Hiroyuki Ohnishi, M.D.,[1] Yukako Kawasaki, M.D.,[2] Masamune Higashigawa, M.D., Ph.D.,[2] Koji Iihara, M.D., Ph.D.,[1] and Susumu Miyamoto, M.D., Ph.D.[3]

[1]Department of Neurosurgery, National Cerebral and Cardiovascular Center, Suita, Osaka; [2]Department of Pediatrics, Yamada Red Cross Hospital, Ise, Mie; and [3]Department of Neurosurgery, Kyoto University Graduate School of Medicine, Kyoto, Japan

The authors report a case of concurrent moyamoya disease and glycogen storage disease Type 1a that was successfully managed with bypass surgery. This 7-year-old Japanese girl, diagnosed with glycogen storage disease Type 1a at the age of 2 years, presented with repeated transient ischemic attacks. Cerebral angiography revealed severe stenosis at the terminal portions of the bilateral internal carotid arteries, with typical moyamoya vessels. The patient underwent superficial temporal artery–middle cerebral artery anastomosis and encephalomyosynangiosis bilaterally, in 2 staged procedures at an interval of 4 months. Despite perioperative administration of glucose, hypoglycemia and metabolic acidosis occurred after both surgeries. The symptoms were milder after the second surgery, in which an increased dose of glucose was used. The patient tolerated the perioperative conditions well under intensified medical treatment, and no further ischemic symptoms occurred. *(DOI: 10.3171/2010.10.PEDS10175)*

Key Words • **moyamoya disease** • **glycogen storage disease Type 1a** • **perioperative complication** • **lactic acidosis**

Moyamoya disease is one of the main causes of childhood ischemic stroke and is characterized by spontaneous progressive stenoocclusive changes of the terminal ICA and fine collateral vessel development at the base of the brain. These conditions are also reported as secondary phenomena of vascular occlusion in several underlying diseases. Glycogen storage disease Type 1a is an autosomal recessive inborn error of carbohydrate metabolism caused by glucose-6-phosphatase deficiency, and the clinical manifestations include growth retardation, rounded doll-like face, hepatomegaly, hypoglycemia, and lactic acidosis.[10] We report on a case of a child with MMD and GSD-1a with a focus on perioperative management.

Case Report

History and Examination. This 7-year-old Japanese girl was examined at her local hospital due to repeated transient ischemic attacks, right hemiparesis, and dysphasia. Magnetic resonance imaging demonstrated no recent ischemic cerebral lesion, but revealed increasing visibility of a fine vascular network around the bilateral carotid fork, suggestive of MMD. The patient's medical history showed that at the age of 2 years, GSD-1a had been suspected after laboratory test results showed lactic acidosis and hypoglycemia. This diagnosis was confirmed by enzymatic assay and molecular analysis. When the patient was 4 years old, sudden-onset left hemiplegia developed following a highly febrile state due to influenza. A brain CT scan revealed an acute right frontoparietal cortical infarction and left frontal subcortical infarction. She was treated conservatively and her left hemiparesis gradually improved.

With the exception of clumsiness in her left hand, the patient's neurological condition and mental development had improved to near-normal levels by the time she was admitted to our institution. The enlarged abdomen was caused by a voluminous soft liver. Laboratory tests revealed elevated levels of aspartate aminotransferase (59 U/L), alanine aminotransferase (75 U/L), total cholesterol

Abbreviations used in this paper: CBF = cerebral blood flow; GSD-1a = glycogen storage disease Type 1a; ICA = internal carotid artery; MMD = moyamoya disease.

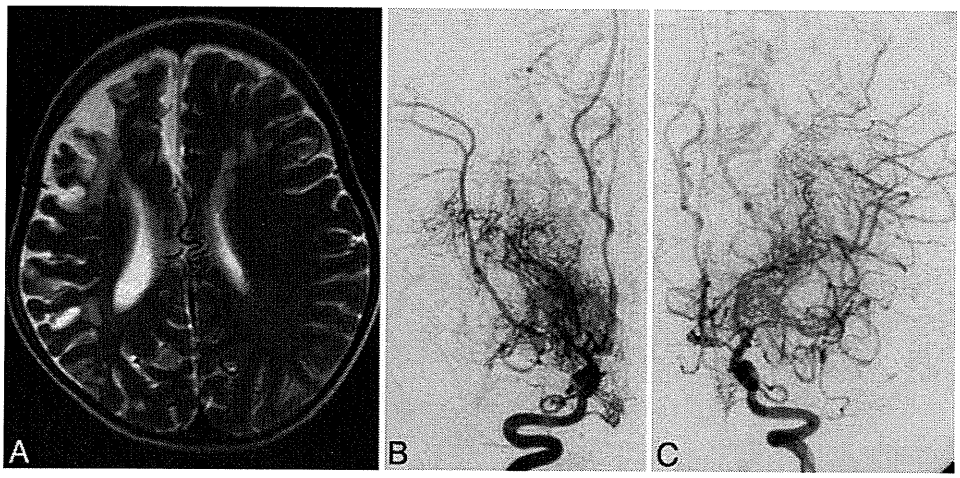

Fig. 1. Images obtained on admission. **A:** Axial T2-weighted MR image showing right frontal cortical infarction with brain atrophy and left frontal white matter infarction. **B and C:** Right **(B)** and left **(C)** ICA angiograms revealing stenosis of the terminal ICA and fine collateral vessel development around the circle of Willis.

(263 mg/dl), triglycerides (1321 mg/dl), lactate (48.3 mg/dl), and uric acid (7.5 mg/dl). The patient's fasting blood glucose level was 74 mg/dl. An MR imaging study was performed; the T2-weighted images showed right frontoparietal cortical atrophy and the previous left frontal subcortical infarction (Fig. 1A). Cerebral angiography demonstrated severe stenosis at the terminal portions of bilateral ICAs, with typical moyamoya vessels at the base of the brain (Fig. 1B and C). There was no obvious abnormality on the posterior circulation or extracranial vasculature. A decrease of CBF in the bilateral frontoparietal region was revealed on SPECT images.

Surgical Treatment and Outcome. Direct revascularization with superficial temporal artery–middle cerebral artery anastomosis and indirect revascularization with encephalomyosynangiosis were performed to prevent further ischemic injury. Bilateral surgery was performed in 2 stages (initially on the left side) with an interval of 4 months. Postoperative angiography revealed a patent bypass; adequate collateral vessels were seen bilaterally (Fig. 2). Postoperative SPECT images showed marked improvement of CBF in regions that preoperatively demonstrated impaired perfusion.

Perioperative Course. Despite continuous pre-, intra-, and postoperative intravenous administration of glucose, hypoglycemia and metabolic acidosis occurred after the first operation. The patient's blood glucose level was 73 mg/dl, the lactate level was 13.0 mmol/L, and the base excess value was −9.1 mmol/L at 3 hours postoperatively; compensatory hyperventilation gradually developed with a respiration rate of 36 breaths per minute and arterial carbon dioxide pressure of 25.6 mm Hg. Hyperventilation ceased following an increased dose of glucose with intravenous infusion of sodium bicarbonate. The patient's respiration rate was 24 breaths per minute and $PaCO_2$ was 35.5 mm Hg at 9 hours postoperatively (Fig. 3). After the second operation, lactic acidosis and compensatory hyperventilation were milder than the first postoperative period because a larger dose of glucose and sodium bicarbonate were administered during the operation and postoperative period. The minimum blood glucose and maximum lactate levels were 82 mg/dl and 10.0 mmol/L, respectively; the minimum base excess was −4.5 mmol/L; and the minimum $PaCO_2$ was 30.0 mm Hg. The patient tolerated each postoperative period well; no further ischemic neurological symptom developed.

Discussion

Moyamoya disease is a cerebrovascular condition that results in the narrowing of vessels at the circle of Willis and collateral vessel formation at the base of the brain.[1] Although these vascular conditions have been reported in association with various diseases, only 2 cases concurrent with GSD-1a have been reported in the literature.[2,11] The pathogenesis of MMD in patients with GSD-1a has not yet been clarified. In an autopsy case of a patient with

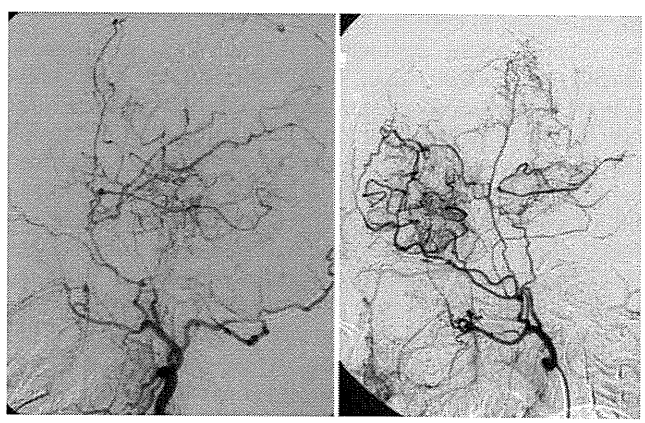

Fig. 2. Images obtained after bilateral bypass surgery. **Left:** Postoperative right external carotid artery angiogram demonstrating adequate development of collateral vessels from encephalomyosynangiosis. **Right:** Postoperative left external carotid artery demonstrating the superficial temporal artery perfusing the recipient cortical artery at the frontal region and development of collateral vessels from encephalomyosynangiosis at the temporal and parietal region.

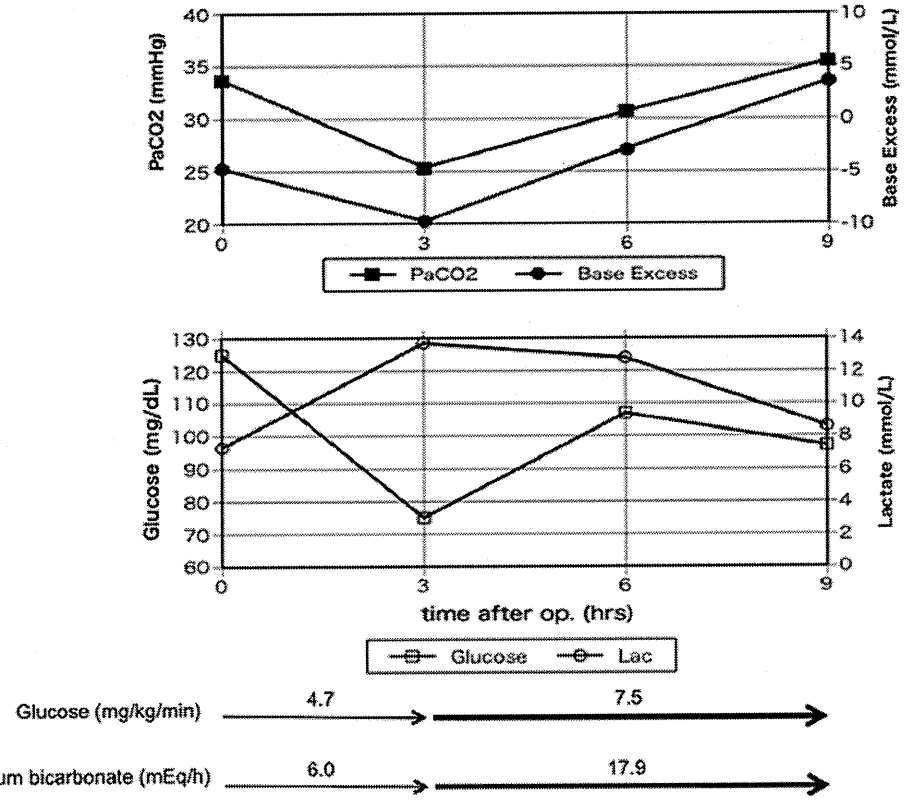

FIG. 3. Graphs showing results of arterial blood gas analysis and glucose levels after the first operation (op). Metabolic acidosis and hypoglycemia were observed at 3 hours postoperatively; compensatory hyperventilation gradually developed. Increasing doses of continuous intravenous infusion of glucose and sodium bicarbonate resolved the metabolic acidosis. Lac = lactate.

GSD-1a and concurrent pulmonary hypertension, Pizzo[9] described pathological changes suggestive of a chronic vasoconstrictive process with intimal fibrosis of the pulmonary vasculature. Similar histopathological findings of intra- and extracranial vessels had been observed in patients with MMD,[3] thus GSD-1a may be a possible cause of MMD. Further studies involving more patients with concurrent MMD and GSD-1a are necessary to elucidate the relationship between these 2 conditions.

The inherent deficiency of glucose-6-phosphatase activity in patients with GSD-1a leads to the inhibition of free glucose release from liver glycogen into the bloodstream, resulting in hypoglycemia. Production of lactate increases, given the normal glycolysis of glucose-6-phosphate. Therefore, patients with GSD-1a tend to exhibit lactic acidosis and hyperventilate to compensate for metabolic acidosis. Lactic acidosis becomes more severe when the glucose supply is exhausted.[7] On the other hand, cerebral cortical vessels in patients with MMD may dilate in response to decreased perfusion pressure caused by bilateral carotid artery stenoocclusive lesions.[6,8] Therefore, cerebrovascular ischemic symptoms of MMD are usually precipitated by hyperventilation via decreased $PaCO_2$. Because the most serious perioperative ischemic complications related to cerebral bypass surgery for MMD are more often caused by the occurrence of perioperative hypo- and hypercapnia than the surgical procedure itself,[4,5] meticulous perioperative management to prevent potentially hazardous lactic acidosis is mandatory. Goutières et al.[2] reported a case of a surgically treated patient with MMD associated with GSD-1a. The patient underwent right encephaloduroarteriomyosynangiosis (EDAMS) and developed complete left hemiplegia at 36 hours postoperatively, but specific causes of ischemic complications were not mentioned. An important lesson learned from the present case is that successful perioperative management after bypass surgery in patients with MMD and GSD-1a depends on meticulous prevention of hypoglycemia and lactic acidosis by sufficient administration of glucose and sodium bicarbonate. Another case, reported by Sunder,[11] involved a 17-year-old boy, who was treated without surgery and suffered episodic headache and transient ischemic attacks. Our case is distinct from previously reported cases in that revascularization surgery under intensified perioperative medical treatment effectively improved CBF and prevented ischemic stroke.

Conclusions

We report on a patient with concurrent MMD and GSD-1a who was managed successfully during her perioperative period. Although surgical risk for MMD may be higher in patients with GSD-1a, surgical revascularization under intensified perioperative management should be considered to prevent future ischemic events.

Disclosure

The authors report no conflict of interest concerning the mate-

rials or methods used in this study or the findings specified in this paper.

Author contributions to the study and manuscript preparation include the following. Conception and design: Egashira. Reviewed final version of the manuscript and approved it for submission: Miyamoto. Administrative/technical/material support: Ohnishi, Kawasaki, Higashigawa. Study supervision: Takahashi, Iihara.

References

1. Fukui M: Current state of study on moyamoya disease in Japan. **Surg Neurol 47:**138–143, 1997
2. Goutières F, Bourgeois M, Trioche P, Demelier JF, Odievre M, Labrune P: Moyamoya disease in a child with glycogen storage disease type Ia. **Neuropediatrics 28:**133–134, 1997
3. Ikeda E: Systemic vascular changes in spontaneous occlusion of the circle of Willis. **Stroke 22:**1358–1362, 1991
4. Iwama T, Hashimoto N, Yonekawa Y: The relevance of hemodynamic factors to perioperative ischemic complications in childhood moyamoya disease. **Neurosurgery 38:**1120–1126, 1996
5. Matsushima Y, Aoyagi M, Suzuki R, Tabata H, Ohno K: Perioperative complications of encephalo-duro-arterio-synangiosis: prevention and treatment. **Surg Neurol 36:**343–353, 1991
6. Nishimoto A, Onbe H, Ueta K: Clinical and cerebral blood flow study in moyamoya disease with TIA. **Acta Neurol Scand Suppl 60 (Suppl 72):**434–435, 1983
7. Nuoffer JM, Mullis PE, Wiesmann UN: Treatment with low-dose diazoxide in two growth-retarded prepubertal girls with glycogen storage disease type Ia resulted in catch-up growth. **J Inherit Metab Dis 20:**790–798, 1997
8. Oku S, Okumura F, Kikuchi H, Karasawa J, Takeuchi S, Nagata I: [The effects of arterial carbon dioxide tension on cerebral blood flow and on cerebral function in "moyamoya" disease.] **J Jpn Soc Clin Anesth 5:**360–368, 1985 (Jpn)
9. Pizzo CJ: Type I glycogen storage disease with focal nodular hyperplasia of the liver and vasoconstrictive pulmonary hypertension. **Pediatrics 65:**341–343, 1980
10. Rake JP, Visser G, Labrune P, Leonard JV, Ullrich K, Smit GP: Glycogen storage disease type I: diagnosis, management, clinical course and outcome. Results of the European Study on Glycogen Storage Disease Type I (ESGSD I). **Eur J Pediatr 161 (Suppl 1):**S20–S34, 2002
11. Sunder TR: Moyamoya disease in a patient with type I glycogenosis. **Arch Neurol 38:**251–253, 1981

Manuscript submitted April 23, 2010.
Accepted October 14, 2010.

Address correspondence to: Yusuke Egashira, M.D., Department of Neurosurgery, Gifu University, Graduate School of Medicine, Yanagido, Gifu-city, Gifu, Japan 501-1194. email: egashi@gifu-u.ac.jp.

Histologic characterization of mobile and nonmobile carotid plaques detected with ultrasound imaging

Takeshi Funaki, MD,[a] Koji Iihara, MD, PhD,[a] Susumu Miyamoto, MD, PhD,[b] Kazuyuki Nagatsuka, MD, PhD,[c] Tomohito Hishikawa, MD, PhD,[a] and Hatsue Ishibashi-Ueda, MD, PhD,[d] *Osaka and Kyoto, Japan*

Objectives: Although mobile plaques in the carotid arteries detected by duplex ultrasound imaging are considered to cause unstable neurologic symptoms such as crescendo transient ischemic attack or progressive stroke, the histology of mobile plaques has not been sufficiently documented. This study examined the histopathologic features of mobile plaques of the carotid artery and compared the histopathology between mobile and nonmobile plaques.

Methods: Of 228 carotid plaques assessed by preoperative carotid ultrasound imaging, 21 (9.3%) were diagnosed as mobile symptomatic plaques. Of these, 18 were intact after excision by endarterectomy and enrolled for histologic examination. From the remaining 207 nonmobile plaque specimens, 17 nonmobile but symptomatic plaque specimens were extracted for histologic comparison. An investigator blinded to the ultrasound findings assessed both plaque specimens for fibrous cap thickness, fibrous cap rupture, fibrous cap area, necrotic core size, inflammatory cells, intraplaque hemorrhage, and mural thrombus. Clinical data, including progressive ischemic symptoms after admission, were also examined.

Results: Progressive ischemic symptoms were more frequently seen in patients with mobile plaques than in those with nonmobile plaques (33.3% vs 0%, $P = .02$). The ratio of the cross-sectional area of the necrotic core to that of the entire plaque was significantly larger for mobile plaques than for nonmobile plaques (mean, 0.660 vs 0.417, $P < .0001$). Mural thrombus was more prevalent among mobile plaques (89%) than among nonmobile plaques (59%), but the difference was not significant ($P = .06$). The median minimum thickness of the fibrous cap was extremely small in both groups (80 μm in mobile plaques and 100 μm in nonmobile plaques, $P = .33$).

Conclusions: The histologic characteristics of mobile carotid plaques are different from those of nonmobile symptomatic plaques, especially in the area of the necrotic core. This histologic difference may partly explain the unstable neurologic presentations of patients with mobile carotid plaques. (J Vasc Surg 2011;53:977-83.)

Mobile components in symptomatic carotid plaques, as detected with a duplex ultrasound scan using the recently developed high-resolution real-time B-mode system, are assumed to cause unstable neurologic symptoms such as crescendo transient ischemic attack or progressive stroke. These types of plaque with mobility have been denoted variously in several case reports as "mobile plaques,"[1] "floating plaques,"[2-4] "mobile thrombi,"[5] or "floating thrombi."[6,7] Some authors have emphasized the high potential of the mobile plaque to cause recurrence of ischemic attacks within a short period.[5,8,9] They have also speculated that plaque disruption and mural thrombus resulted in mobile plaques.[5,6]

Previous reports have not, however, sufficiently documented the mechanism of that mobility or the histologic feature of such plaques. We hypothesized that certain histologic differences may exist between mobile and nonmobile symptomatic carotid plaques as long as clinical symptoms caused by mobile plaques are more unstable than those by nonmobile plaques. To confirm this hypothesis, we compared the prevalence of several histologic factors between mobile and nonmobile plaques in symptomatic patients, with the examination of clinical data including progressive ischemic symptoms after admission.

METHODS

This study was performed in accordance with the ethical guidelines of our institution and included patients' informed consent.

Plaque selection. Between April 2003 and March 2008, 228 carotid plaques were excised by carotid endarterectomy (CEA) at the National Cerebral and Cardiovascular Center, Osaka, Japan. All patients had been assessed with preoperative carotid ultrasound imaging, and 21 symptomatic patients (9.3%) had been diagnosed with mobile plaques. The study excluded 3 of 21 mobile plaque specimens after the histologic examination because they

From the Department of Neurosurgery,[a] Cerebrovascular Division, Department of Medicine,[c] and Department of Pathology,[d] National Cerebral and Cardiovascular Center, Osaka; and Department of Neurosurgery, Kyoto University Graduate School of Medicine, Kyoto.[b]

Competition of interest: none.

Additional material for this article may be found online at www.jvascsurg.org.

Reprint requests: Takeshi Funaki, MD, Department of Neurosurgery, Kyoto University Graduate School of Medicine, 54 Kawahara-cho and Shogoin, Sakyo-ku, Kyoto, Japan (e-mail: funaki1103@gmail.com).

The editors and reviewers of this article have no relevant financial relationships to disclose per the JVS policy that requires reviewers to decline review of any manuscript for which they may have a competition of interest.

0741-5214/$36.00

doi:10.1016/j.jvs.2010.10.105

were damaged during plaque excision. From the remaining 207 nonmobile plaques, 20 symptomatic plaques were randomly extracted for histologic comparison. After the histologic examination, the study excluded 3 of the 20 nonmobile plaque specimens because they were too damaged. The remaining 35 plaque specimens, comprising 18 mobile plaques and 17 nonmobile plaques, were used in this study.

Clinical data. We reviewed clinical data of the 35 patients with excised plaques. Their symptoms at admission were classified into four categories: amaurosis fugax, transient ischemic attack (TIA), transient symptom associated with infarction (TSI), and stroke. Amaurosis fugax was defined as a transient ipsilateral blindness or visual field defect. TIA was defined as a transient neurologic symptom that lasts <24 hours without any evidence of brain infarction confirmed by diffusion-weighted images (DWI) in magnetic resonance imaging. TSI was defined as a transient neurologic symptom that lasts <24 hours with evidence of brain infarction, which is supposed to have higher in-hospital recurrent ischemic rate than TIA.[10] Stroke was confirmed by positive findings in the territory of the ipsilateral carotid artery on DWI. Progressive symptoms were also recorded when the patient experienced a recurrence and worsening of neurologic symptoms after admission, with an increase of ischemic lesions confirmed by DWI.

The degree of carotid stenosis was measured by digital subtraction angiography according to the method used in the North American Carotid Surgery Trial.[11] The other clinical data recorded were age, sex, treatment for hypertension, treatment for diabetes, treatment for hyperlipidemia, smoking within the preceding year, statin administration, and aspirin administration. Median intervals from the last ischemic event to CEA and then from the last ultrasound imaging to CEA were also examined.

Ultrasound imaging. All patients underwent preoperative carotid ultrasound scanning ≤1 month before CEAs using a commercially available, real-time 2-dimensional device equipped with a 7.5-MHz transducer. B-mode scans, B-mode scans with color Doppler imaging, and pulsed-Doppler scans were routinely performed. If a stroke physician suspected the presence of mobile plaques on duplex ultrasound imaging, the images would be recorded as video files. Two skilled stroke physicians, who had no previous knowledge of the patient's clinical information, including a coauthor (K.N.), reviewed video files and made a final diagnosis of mobile plaques. The findings of the mobile plaques were defined and classified as follows:

1. Mobile components that are localized at the surface of the plaque and that rise and fall in a manner inconsistent with or exceeding arterial pulsatile wall motion (jellyfish sign[12]),
2. Mobile components inside the plaque that change slowly and irregularly like viscous liquid (liquefaction sign),
3. Movements localized within an ulcer's inner surface (Fig 1; Video 1, online only), and

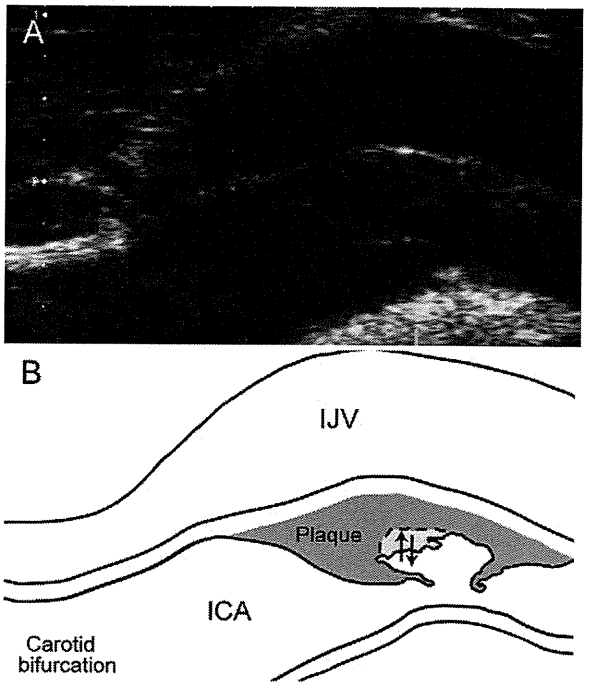

Fig 1. A, A longitudinal duplex ultrasound image of a mobile plaque demonstrates an ulcerated plaque in the extracranial internal carotid artery. **B**, A schema representing the mobile component in the plaque: an ulcer's inner surface rose and fell according to the pulsation, as indicated with *arrows,* which was defined as "movements localized within an ulcer's inner surface" (see also Video 1, online only). *ICA,* Internal carotid artery; *IJV,* internal jugular vein.

4. Movements of protuberances (Fig 2; Video 2, online only).

Plaque excision. General anesthesia was initiated, and CEA was performed using an operating microscope and somatosensory evoked potential monitoring to selectively place the shunt. For some cases with a mobile plaque, each surrounding artery (including the common, external, and internal carotid arteries) was clamped as soon as it was exposed to minimize the risk of distal embolism caused by the manipulation of the internal carotid artery. Upon cross-clamping, the common carotid artery was incised with scalpels to determine the dissection plane, usually made at the level of the internal elastic membrane, under the operating microscope. A microdissector was inserted meticulously, not to disturb the cleavage plane, until the distal end of the plaque and the patent lumen of the distal internal carotid artery were ascertained. The distal and proximal edges of the plaque were cut and finally pulled out from the orifice of the external carotid artery. In this way, most of the carotid plaque could be removed en bloc with minimum surgical trauma. If a cut penetrated the surface of the specimen to the lumen, it could be judged in the histologic examination that the cleavage resulted from surgical trauma, not plaque rupture.

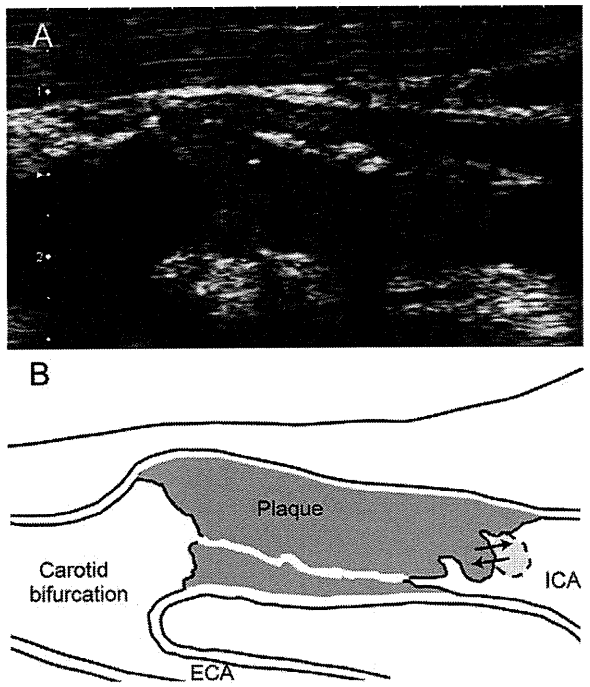

Fig 2. A, A longitudinal duplex ultrasound image demonstrates a massive mobile plaque almost occluding the internal carotid artery (*ICA*) and a protuberance from the distal end of the plaque. **B**, A schema representing the shaking movement of the protuberance (*arrows*): the original video also revealed a mobile component inside the plaque that changed slowly and irregularly like viscous liquid (liquefaction sign, see also Video 2, online only). *ECA*, External carotid artery.

Histopathology. The excised plaques were immediately fixed in Histochoice fixative (Amresco, Cleveland, Ohio) for 48 hours and decalcified by ethylenediaminetetraacetic acid (EDTA). To preserve the immunoreactivity, we used Histochoice for fixation and EDTA for decalcification of specimens before embedding in paraffin blocks.[13] Each plaque was sectioned transversely at the carotid bifurcation, and further sections were taken at 5-mm intervals along the length of internal carotid arteries for embedding in paraffin.[14] Adjacent 5-μm transverse sections were stained with hematoxylin and eosin, elastin van Gieson, Masson trichrome, and von Kossa. When a certain section seemed near the plaque rupture site, additional subserial slices were performed to avoid skipping focal instability. For immunohistochemistry analyses, we performed immunostaining for T cell (CD3, DAKO, Glostrup, Denmark), macrophages (CD68, DAKO). Immunostaining with glycophorin A (CD235a, DAKO) was also performed to detect intraplaque hemorrhage.[15] An experienced cardiovascular pathologist (H.I.) histologically examined all sections without any knowledge of clinical details and findings of carotid ultrasound imaging.

The histologic features of plaques assessed in this study were minimum cap thickness, prevalence of the rupture of fibrous cap and ulceration, necrotic core size, quantity of inflammatory cells (including macrophages and lymphocytes), degree of intraplaque hemorrhage, and prevalence of mural thrombus. Minimum cap thickness was defined as the thinnest part of the fibrous cap in total cross-sections of each plaque measured by a manometer attached to the microscope.[16] Plaque rupture, a break in the fibrous cap, was recorded when there was clear interaction between the lipid core and the lumen, usually at a point of thinning and inflammation and when the break in the cap did not seem to have been created during surgery (Fig 3, *A*). A necrotic core was defined as an amorphous material containing cholesterol crystals (Fig 3, *B*).[17]

To measure the area of necrotic core, we sampled three cross-sections: on the carotid bifurcation, 5 mm distal to the bifurcation, and 10 mm distal to the bifurcation. On each cross-section, the necrotic core and the entire plaque area were measured by WinROOF 5.0 morphometry software (Mitani Co, Kanazawa, Japan), and the ratio of the mean cross-sectional area of the necrotic core to that of the entire plaque area was calculated. We also measured the actual area of the fibrous cap for mobile and nonmobile plaques on the three cross-sections, and the median value of the fibrous cap area in each plaque was calculated.

A "recent" intraplaque hemorrhage was recorded when an area of erythrocytes within the plaque caused disruption of plaque architecture, whereas an "old" intraplaque hemorrhage was recorded when evidence showed organized hemorrhage with the accumulation of hemosiderin-laden macrophages or iron deposits on plaque connective tissue.[18] Old intraplaque hemorrhage was also recorded when the ratio of the glycophorin A-positive area to the whole plaque area was >40%. Plaque inflammation with macrophage and lymphocyte infiltration was recorded according to the number of CD68-negative or CD3-positive cells: infiltration of >20 inflammatory cells in the fibrous cap was defined as positive inflammation to the fibrous cap. Mural thrombus was defined as a fibrin organization of the endothelium or the fibrous cap of plaques (Fig 3, *C*).

Statistical analysis. Patients with mobile plaques and those with nonmobile plaques were compared for baseline characteristics, the prevalence of progressive symptoms, and plaque histologic features using a *t* test, the Wilcoxon rank sum test, or the Fisher exact test, as appropriate. Two-sided values of $P < .05$ were considered significant. Statistical analysis was performed with JMP 7.12 software (SAS Institute, Cary, NC).

RESULTS

Patients displaying mobile plaques and nonmobile plaques exhibited no significant difference in age, sex, diabetes mellitus, hyperlipidemia, smoking, coronary artery disease, administration of statins, administration of aspirin, or degree of stenosis (Table I). All statins were administrated with the usual doses (atorvastatin ≤20 mg, pravastatin ≤20 mg, or pitavastatin ≤2 mg), and no patients received high-dose statin therapy. Hypertension was observed more frequently in patients with nonmobile plaques.

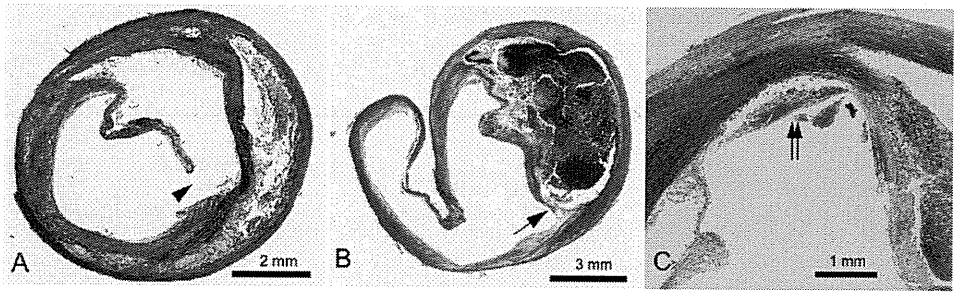

Fig 3. An example of histologic features of a mobile plaque (the same plaque as shown in Fig 1). **A**, A photomicrograph of the carotid bifurcation (Masson's trichrome staining, original magnification ×1) demonstrates complete disruption of the fibrous cap (*arrowhead*). **B**, Another cross-section (Masson's trichrome staining, original magnification ×1) demonstrates a large necrotic core with a fresh intraplaque hemorrhage (*asterisk*), which was covered with thin fibrous cap (*arrow*). **C**, A photomicrograph (Masson's trichrome staining, original magnification ×2) shows intramural fibrin deposit, indicating mural thrombus (*double arrow*).

Table I. Clinical characteristics at the time of carotid endarterectomy of study patients

Characteristics	*Mobile plaques (n = 18)*	*Nonmobile plaques (n = 17)*	P
Age, mean (SD), year	70.8 (11.5)	66.2 (8.7)	.19
Female, No. (%)	3 (16.7)	1 (5.9)	.60
Stenosis, mean (SD), %	73.2 (24.4)	76.5 (15.2)	.63
Risk factors, No. (%)			
Hypertension	11 (61.1)	17 (100)	.01
Diabetes mellitus	4 (22.2)	7 (41.2)	.29
Hyperlipidemia	11 (61.1)	12 (70.6)	.72
Smoking	9 (50.0)	13 (76.5)	.16
Medications, No. (%)			
Statin	7 (38.9)	7 (41.2)	1.00
Aspirin	10 (55.6)	13 (76.5)	.29
Interval to CEA, median (IQR) days			
From last ischemic event	12.5 (7.5-26.75)	33 (13.5-70.5)	.01
From last ultrasound study	3 (1-8.25)	9 (3.5-21.5)	.03
MRI-DWI positive, No. (%)	14 (77.8)	14 (82.4)	1.00

DWI, Diffusion-weighted image; *IQR,* interquartile range; *MRI,* magnetic resonance imaging; *SD,* standard deviation.

The median interval from the last ischemic event to CEA was 12.5 days (maximum, 41 days) in patients with mobile plaques, and the interval between the onset of symptoms and CEA, as well as that between ultrasound imaging and CEA, was significantly longer in patients with nonmobile plaques. No patients in this study had atrial fibrillation or other embolic sources. The incidence of the acute cerebral infarction detected with preoperative DWI did not show significant difference between mobile and nonmobile plaques (77.8% vs 82.4%, $P > .99$).

Clinical symptoms. The first ischemic symptoms among the 18 patients with mobile plaques were cerebral infarct in 11 patients, TSI in 5, TIA in 1, and amaurosis fugax without positive DWI finding in 1. Symptoms among 17 patients with nonmobile plaques included cerebral infarct in 6, TSI in 6, TIA in 3, and amaurosis fugax without positive DWI finding in 2. Progressive symptoms after admission were observed in six patients (33.3%) with mobile plaques, whereas no progression was seen in the patients with nonmobile plaques ($P = .02$).

Histologic features. All histologic features in mobile plaques and nonmobile plaques are summarized in Table II. The ratio of the mean cross-sectional area of the necrotic core to that of the entire plaque area was significantly larger in mobile plaques than in nonmobile plaques (mean, 0.660 vs 0.417, $P < .0001$).

Plaque ruptures were seen in 83% of mobile plaques. The median minimum cap thickness was 80 μm, which is smaller than that considered to be the critical value of minimum cap thickness for cap rupture.[16] There were no significant differences in the prevalence of cap rupture (83% vs 82%) or median minimum cap thickness (80 vs 100 μm) between mobile plaques and nonmobile plaques. The median area of the fibrous cap was, however, significantly smaller in the mobile plaques than in nonmobile plaques (9200 vs 15,900 μm^2; $P = .02$).

Although mural thrombus was more prevalent in mobile plaques (89%) than in nonmobile plaques (59%), the difference was not significant ($P = .060$). There was also no significant difference between mobile and nonmobile